



# Monitoring cyanobacterial harmful algal blooms at high spatiotemporal resolution by fusing Landsat and MODIS imagery

Yongquan Zhao<sup>a</sup>, Desheng Liu<sup>a,\*</sup>, Xiaofang Wei<sup>b</sup>

<sup>a</sup> Department of Geography, The Ohio State University, 1036 Derby Hall, 154 North Oval Mall, Columbus, OH 43210-1361, United States

<sup>b</sup> Department of Water Resources Management, Central State University, Wilberforce, OH 45384, United States



## ARTICLE INFO

### Keywords:

Cyanobacteria-rich harmful algal blooms (CyanoHABs)  
Broad wavelength algae index (BWA)  
Spatial-temporal image fusion (STIF)  
Landsat  
MODIS

## ABSTRACT

Toxic Cyanobacteria-rich Harmful Algal Blooms (CyanoHABs) are severe environmental issues impacting water environment, aquatic life populations, and surrounding wild and human lives. Given their fast-changing variations in space and time, frequent monitoring of CyanoHABs with sufficient spatial details and coverage is needed to understand their impacts. However, current monitoring activities based on *in situ* or satellite data do not meet this requirement due to the limited spatial coverages of buoy measurements and the compromise between spatial resolution and temporal frequency of satellite observations. In this study, we develop a Spatial-Temporal Image Fusion (STIF) approach to enable high spatial-temporal resolution monitoring of CyanoHABs. The proposed approach consists of two steps: (1) a new CyanoHAB spectral index called Broad Wavelength Algae Index (BWA) is developed for fine-but-sparse (Landsat) and coarse-but-frequent (MODIS) satellite images, and (2) the Landsat and MODIS derived BWA images are fused by the Robust Adaptive Spatial and Temporal Fusion Model (RASTFM) to generate fine-and-frequent Landsat-like BWA images. Our results show that the proposed BWA index is with higher similarity and correlation with the reference Cyanobacteria Index (CI) images and *in situ* observations than the comparative algae indices devised for broad wavelength sensors. Moreover, the 30-m Landsat-like BWA image series provide more accurate and detailed results than their 500-m MODIS counterparts and greatly improve the temporal frequency over Landsat-based algae indices, demonstrating the contribution of the improved spatial-temporal resolution achieved by the proposed STIF approach. Consequently, this research fills the gap of high spatiotemporal resolution monitoring of CyanoHABs and paves a new way of assessing water environment in a timely and detailed manner.

## 1. Introduction

Toxic Cyanobacteria-rich Harmful Algal Blooms (CyanoHABs) are severe water environmental problems for global inland water bodies concomitant to the growing discharge of domestic or industrial wastewater as well as agriculture and fertilizer runoff (Glibert et al., 2005). The blooms not only deplete the dissolved oxygen in waters that result in mass death to water lives but also release toxins, e.g., microcystin, that cause health risks to wildlife, livestock, pets, and humans due to CyanoHABs exposure (Hallegraeff, 1993). Furthermore, surface foams or scums formed by CyanoHABs and their odorous compounds foul up water quality and surrounding recreational environment (Anderson et al., 2002). Additionally, CyanoHABs are with fast-changing characteristics in space and time because of hydrodynamics and many environmental factors, e.g., eutrophication degrees, water temperature, solar illumination, wind stress (Michalak et al., 2013; Wynne et al., 2010). Hence, quantifying the detailed spatial distribu-

tions of CyanoHABs in inland water bodies on a regular and frequent basis is of great significance and importance, which requires high spatial-temporal resolution monitoring abilities.

CyanoHABs have long been monitored through sensors deployed on buoys to continuously measure various CyanoHAB proxy pigments such as chlorophyll-a (Chl-a) and phycocyanin (PC). However, the spatial distribution of monitoring buoys is usually quite limited over large water bodies because of high installation and maintenance costs in practice (Babin et al., 2008). Therefore, buoy-based observation systems do not provide spatially continuous observations and have limited geographical coverage, especially for large water bodies (Kutser, 2009). Given that, satellite remote sensing has been used as a more comprehensive and cost-effective way to complement the limitations of buoy-based observation systems (Matthews, 2011), thereby providing a synoptic view of CyanoHABs' dynamics and life cycles (emergence, growth, senescence, and death) (Wynne et al., 2013).

Existing remote sensing approaches for algal bloom delineation from satellite imagery include single band algorithms (Kutser, 2009),

\* Corresponding author.

E-mail address: [liu.738@osu.edu](mailto:liu.738@osu.edu) (D. Liu).

analytical algorithms (Stumpf et al., 2016), band ratio algorithms (Matthews, 2011), and baseline algorithms (Stumpf et al., 2016). Single band algorithms utilize a single feature band of algal blooms to map cyanobacterial extent or biomass (Galat and Verdin, 1989; Ho et al., 2017; Kutser et al., 2006). Analytical models (Kutser, 2004; Simis et al., 2005) utilize multi- or hyper-spectral satellite images to solve backscatter and absorption caused by different substances that are optically active and then map CyanoHAB pigments quantitatively. Band ratio algorithms can be applied to both coarse- and fine-resolution satellites (Kutser, 2009) but they are more commonly used for sensors with a few wide wavelength bands, e.g., Landsat, SPOT, and IKONOS (Matthews, 2011; Stumpf et al., 2016). Band ratios are either directly derived from two spectral bands (Gitelson et al., 1993; Lathrop, 1992; Mayo et al., 1995; Vincent et al., 2004; Yacobi et al., 1995) or calculated as the normalized difference images of two spectral bands (Mishra and Mishra, 2012; Oyama et al., 2015). However, single band, analytical, and band ratio (especially for ratios directly derived from two bands) algorithms require accurate atmospheric correction to obtain water reflectance and are sensitive to sun-glint effects (Stumpf et al., 2016), which could lead to large biases in results without accurate water-leaving reflectance (Wang and Shi, 2007). In contrast, baseline algorithms utilize more than two spectral bands to calculate the second derivative by measuring a reflectance peak height of the spectral feature band(s) of algal blooms above a baseline determined by its/their two adjacent bands at shorter and longer wavelengths (Stumpf et al., 2016; Stumpf and Werdell, 2010). Since the second derivative calculation can remove the effects of mild sun-glint and atmosphere (Hu et al., 2012; Philpot, 1991), baseline algorithms are more robust than the former three types of methods and are thus widely used in algal bloom monitoring studies (Clark et al., 2017; Lunetta et al., 2015; Wynne et al., 2010). To date, a number of spectral indices have been developed using baseline algorithms for different satellite sensors at various spatial and temporal resolutions (Stumpf et al., 2016), including Fluorescence Line Height (FLH) based on MODIS (Letelier and Abbott, 1996), Maximum Chlorophyll Index (MCI) based on MERIS (Gower et al., 2005), Floating Algae Index (FAI) based on Landsat and MODIS (Hu, 2009), Cyanobacteria Index (CI) based on MODIS and MERIS (Wynne et al., 2013; Wynne et al., 2008), and Maximum Peak-Height (MPH) based on MERIS (Matthews et al., 2012).

While extensive studies have been conducted to monitor algal blooms using multiple satellite sensors across various water bodies, they are all subject to the trade-off between spatial and temporal resolution of satellite sensors (Kutser, 2009; Zhao and Huang, 2017). On one hand, coarse-but-frequent sensors such as Terra/Aqua MODIS provide daily observations but with coarse spatial resolutions (e.g., 250-m to 1000-m) that cannot reveal spatial details of CyanoHABs or delineate CyanoHABs in small lakes. On the other hand, fine-but-sparse sensors such as Landsat-8 OLI can provide more spatial details of algal blooms with their fine-resolution pixels (e.g., 30-m), but their long revisit cycle (e.g., 16 days) makes them insufficient to capture the temporal dynamics of algal blooms (Yacobi et al., 1995). Therefore, existing methods can only monitor algal blooms either in a coarse but timely manner or a fine but less frequent manner, thereby failing to monitor CyanoHABs with high spatiotemporal resolution (Kutser, 2009). As a solution to the lack of frequent fine-resolution Earth observations, Spatial-Temporal Image Fusion (STIF) can fuse coarse-but-frequent and fine-but-sparse satellite images to generate fine-and-frequent image series in an effective and low-cost way (Gao et al., 2006; Zhao et al., 2018b). STIF methods utilize spatial detail and temporal change information from prior fine-but-sparse images and coarse-but-frequent images, respectively (Zhu et al., 2016).

Recently, STIF has been used for high spatiotemporal resolution monitoring of water quality, such as Chl-a, turbidity, and total suspended solid, by blending fine-but-sparse (Landsat) and coarse-but-frequent (MODIS) water-leaving reflectance images (Dona et al., 2015; Swain and Sahoo, 2017) with the widely used Spatial and Temporal

Adaptive Reflectance Fusion Model (STARFM, Gao et al., 2006). These STIF-based water quality studies work well for downscaling non-spatial changes but perform less effectively when dealing with spatial changes (Zhao et al., 2018b), such as the patchy surface scums formed by CyanoHABs. Moreover, the existing algae delineation methods based on fine-resolution broad band satellite imagery, e.g., Landsat, do not consider the interference from water suspended sediments, which would lead to overestimation of cyanobacteria loadings if waters have high suspended sediment loadings (Kutser, 2009).

The purpose of this study is to develop a STIF approach to enable high spatial-temporal resolution monitoring of CyanoHABs in western Lake Erie where CyanoHABs have been boosted due to the invasion of Zebra mussels since the 1990s (Wynne et al., 2013). Our proposed STIF approach will fuse observations from fine-but-sparse satellites with broad wavelength (e.g., Landsat) and coarse-but-frequent satellites (e.g., MODIS) to detect CyanoHABs at high spatiotemporal resolution through the following two steps. First, we develop a new baseline-based CyanoHAB spectral index called Broad Wavelength Algae Index (BWAII) based on Landsat and MODIS observations, which can mitigate the interference of water suspended sediments when detecting CyanoHABs. Then, we apply the Robust Adaptive Spatial and Temporal Fusion Model (RASTFM; Zhao et al., 2018b) to generate fine-and-frequent Landsat-like BWAII images by fusing the Landsat-derived BWAII images (fine-but-sparse) and MODIS-derived BWAII images (coarse-but-frequent), which can downscale the changes of subsurface algal blooms and floating scums simultaneously. Accordingly, qualitative and quantitative evaluations of the experimental results of the two steps are conducted based on representative algae delineation indices and *in situ* PC and Chl-a concentration data. In the rest of the paper, we will demonstrate the study area and data sources in Section 2, introduce the methodologies and validation criteria in Section 3, describe the experimental results, discussion, and conclusions in Sections 4–6, respectively.

## 2. Study area and data sources

### 2.1. Study area

Lake Erie is the twelfth largest lake in the world (in area) and the fourth largest among the Laurentian Great Lakes, it is also the shallowest, warmest, and most biologically productive lake in the Great Lakes (ODNR, 2016). Moreover, Lake Erie has been experiencing extensive CyanoHABs since the 1960s because of excess phosphorus from surround point and non-point sources and the emergence of invasive Zebra mussels in the 1990s (Michalak et al., 2013; Wynne et al., 2013). CyanoHABs generally break out in the west basin of Lake Erie and spread to the central and east parts gradually. Hence, western Lake Erie is selected as our study area for CyanoHAB monitoring at high spatiotemporal resolution (see Fig. 1). In this study, we focus on the CyanoHABs in 2017 because the *Microcystis* cyanobacteria blooms in 2017 had a severity index of 8 (NOAA, 2019), indicating quite severe blooms. Moreover, there are two types of data sources including real-time *in situ* PC and Chl-a concentration data from buoys and surface reflectance images from satellites.

### 2.2. Real-time *in situ* PC and Chl-a concentration data

PC and Chl-a were adopted as CyanoHAB pigments because they are sensitive proxies of CyanoHABs in fresh waters and have been intensively used in CyanoHAB detection studies (Stumpf et al., 2016), and both of the pigments can be detected by Landsat observations directly or indirectly (Mayo et al., 1995; Vincent et al., 2004). Additionally, PC is a light-harvesting pigment that exists in cyanophytes ubiquitously (Ho and Michalak, 2015; Vincent et al., 2004), which is important to be indicated for the CyanoHABs in Lake Erie that are generally dominated by cyanobacteria, e.g., *Microcystis* (Ho and Michalak, 2015). Real-time PC and Chl-a concentrations in Relative Fluorescence Units (RFU) with

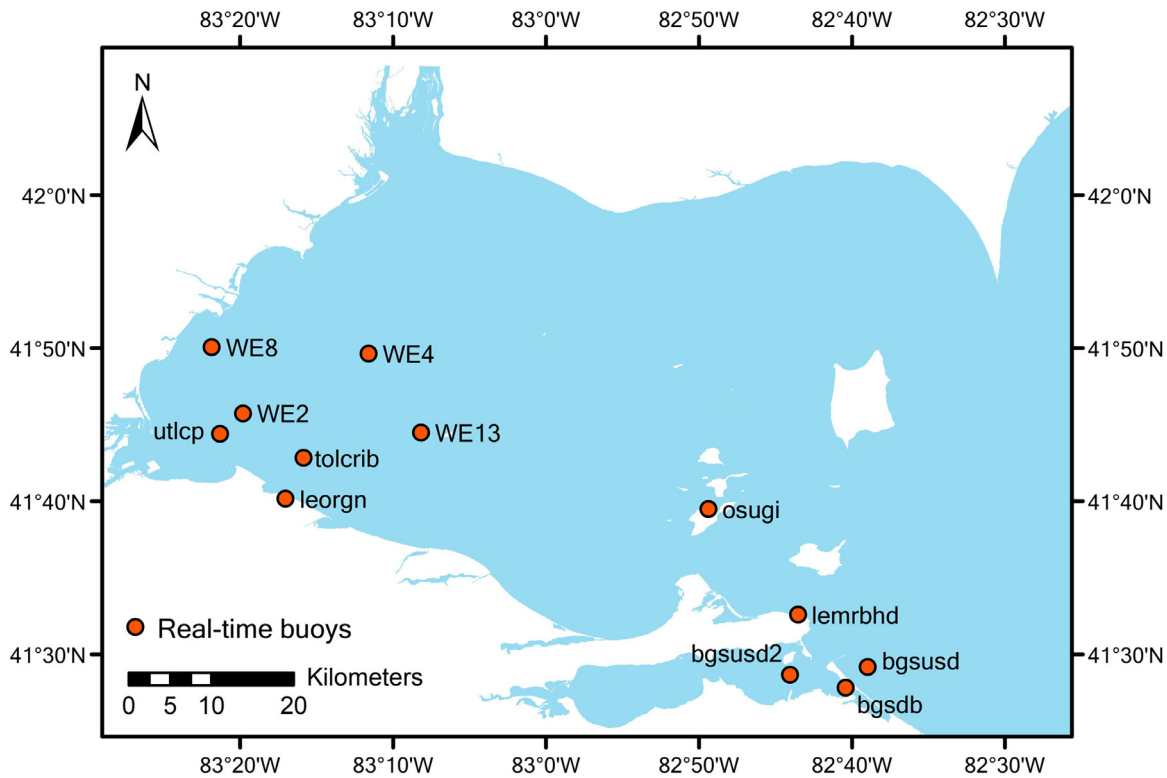


**Fig. 1.** The 12 real-time monitoring stations in western Lake Erie.

synchronous satellite observations from the 12 buoys in Fig. 1 were collected from the HABS Data Portal (<http://habs.glos.us/stations/>) and the Great Lakes Buoy Portal (<https://glbuoys.glos.us/>). The 12 stations measure water environmental parameters every 10 or 15 min. The *in situ* PC and Chl-a data were used for two purposes: one for validating the proposed CyanoHAB spectral index, the other for evaluating the high spatiotemporal resolution CyanoHAB index images generated by STIF. Since the operating time frames of the 12 buoys are different, and the observations could be interfered by noises or even abnormal owing to unexpected reasons, part of the *in situ* buoy data are not available on some dates. Their data availability can be seen in Table A1 of the Appendix. The buoy data on the 16 dates from July to October in 2017 were selected because: (1) the 12 buoys on these dates are with cloud-free Landsat-7 ETM+, Landsat-8 OLI, and MODIS observations in part or in whole, and (2) all the buoys were operated on the 16 dates.

### 2.3. Landsat and MODIS imagery

Landsat and MODIS observations were adopted as fine- and coarse-resolution satellite data for three reasons: (1) they have been widely used to delineate the concentration and spatial distributions of CyanoHABs in inland waters (Hu et al., 2010; Vincent et al., 2004); (2) both sensors have long-term and continuous observations for decades, thereby benefiting the long-term time series analysis of CyanoHABs in western Lake Erie; (3) they have similar band configurations, orbital parameters, near-nadir viewing-solar geometries, and imaging time, thereby providing a solid basis for the STIF processing (Gao et al., 2006). The widely used Landsat and MODIS surface reflectance image products were employed in our experiments.

Firstly, 30-m Landsat surface reflectance products from the USGS EarthExplorer (<https://earthexplorer.usgs.gov/>) were used as fine-resolution data sources. The involvement of ETM+ was to make full use of valid 30-m resolution images even if ETM+ has the SLC-

off problem. Secondly, 500-m Aqua MODIS surface reflectance products (MYD09) were used as coarse-resolution data sources due to the more significant and longer sensor degradation (Lyapustin et al., 2014) and larger instrument calibration changes (Levy et al., 2013) of the Terra MODIS than Aqua MODIS. The MYD09 datasets were downloaded from the Level-1 and Atmosphere Archive & Distribution System Distributed Active Archive Center (LAADS DAAC, <https://ladsweb.modaps.eosdis.nasa.gov/>), and projected onto the same map coordinates with Landsat images (UTM coordinate system under the WGS-84 datum) by the MODIS Reprojection Tool Swath (MRT Swath) software. Moreover, all MODIS images were geometrically matched with Landsat images by applying optimal offsets (Gevaert and García-Haro, 2015), and all MODIS and Landsat images were clipped based on Fig. 1 to obtain western Lake Erie subsets.

The adopted common bands of MODIS and Landsat are shown in Table 1. Note that the Short-Wave InfraRed (SWIR) band of MODIS is chosen as 1230–1250-nm because it is the first choice for algae index derivation such as FAI (Hu, 2009), and the SWIR band between 1628 and 1652-nm is a suggested alternative in the absence of the band between 1230 and 1250-nm (Hu, 2009). The image sizes of the 30-m Landsat and 500-m MODIS images are 2637 × 3128 and 159 × 188, respectively, and the 500-m MODIS bands were resampled to 2637 × 3128 using the nearest neighbor image resampling method.

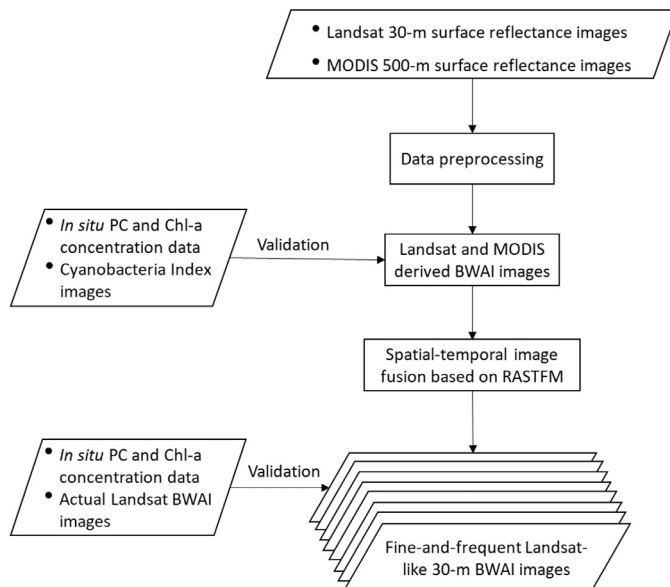
### 3. Methodologies and validation

Fig. 2 demonstrates the workflow of the proposed method for high spatiotemporal resolution monitoring of CyanoHABs in western Lake Erie. First, the CyanoHAB spectral index, i.e., BWAI, is developed for both fine-but-sparse (Landsat) and coarse-but-frequent (MODIS) satellite images. Then, fine-and-frequent Landsat-like BWAI image series are generated by RASTFM based on fine-but-sparse and coarse-but-frequent BWAI images.

**Table 1**

The adopted common bands and central wavelengths (nm) of MODIS, ETM+, and OLI sensors.

MODIS		ETM+		OLI	
Band	Central	Band	Central	Band	Central
B3 Blue: 459 - 479	469	B1 Blue: 450 - 515	482.5	B2 Blue: 450 - 515	482.5
B4 Green: 545 - 565	555	B2 Green: 525 - 605	565	B3 Green: 525 - 600	562.5
B1 Red: 620 - 670	645	B3 Red: 630 - 690	660	B4 Red: 630 - 680	655
B2 NIR: 841 - 876	859	B4 NIR: 775 - 900	837.5	B5 NIR: 845 - 885	865
B5 SWIR: 1230 - 1250	1240	B5 SWIR 1: 1550 - 1750	1650	B6 SWIR 1: 1560 - 1660	1610

**Fig. 2.** The workflow of high spatiotemporal resolution monitoring for CyanoHABs in western Lake Erie.

### 3.1. Data preprocessing

Since many types of datasets are employed in our study, data preprocessing is required to make the inputs ready for the following processing and analysis. For *in situ* PC and Chl-a concentration data, negative values are removed, and daily average values of each station are calculated to mitigate observing noises or errors. The percentage of the retained data is 93.6%. For Aqua MODIS, Landsat-7 ETM+, and Landsat-8 OLI surface reflectance images, clouds are masked based on a threshold method regarding the blue band (Hagolle et al., 2010). Additionally, the Landsat quality assessment bands are used to mask out abnormal values and clouds further. Furthermore, invalid pixels in ETM+ and MYD09 band 5 images are removed because of the ETM+ SLC-off problem and MODIS random scanning errors. Moreover, water bodies in MODIS and Landsat are extracted by the Modified Normalized Difference Water Index (MNDWI; Xu, 2006) because it can suppress built-up land, terrestrial vegetation, and soil noises when extracting water information.

### 3.2. Developing a CyanoHAB index for Landsat and MODIS imagery

The common spectral feature bands of Landsat and MODIS regarding CyanoHABs are the bases to developing an effective CyanoHAB spectral index for the two satellites. CyanoHABs appear similar to terrestrial vegetation, but they have differences and similarities in terms of their feature bands (Kutser, 2009). First, CyanoHABs would have reflectance peaks at the Near-Infrared (NIR) band when there are floating scums/mats formed by CyanoHABs (Hu et al., 2010), especially for algal blooms with high biomass in hypertrophic waters. Second, CyanoHABs have strong reflectance at the green band like ter-

restrial vegetation regardless the reflectance peak at the NIR band (Gitelson, 1993; Mayo et al., 1995). Hence, the green band is a good feature band for detecting algal blooms without floating scums/mats because such blooms have high reflectance at the green band rather than the NIR band. Besides, CyanoHABs have a reflectance peak near 700-nm caused by the combined effect of high scattering and fluorescence of phytoplankton at the red and NIR spectra (Gitelson, 1993; Kutser, 2009). Additionally, CyanoHABs have a typical absorption feature around 620-nm caused by phycocyanin (Kutser, 2004). However, Landsat does not have such band configurations (620- and 700- nm) that can capture the spectral features (Vincent et al., 2004). Hence, detecting reflectance peaks at green or NIR bands is feasible for CyanoHAB delineation with broad wavelength satellites such as Landsat.

However, water suspended sediments generally cause interferences to the green or NIR reflectance of algal blooms (Ritchie et al., 2003). Higher water suspended sediment loadings will give rise to higher water-leaving reflectance, and the maximum reflectance will shift towards longer wavelengths with increasing water turbidity (Goodin et al., 1993). Therefore, we devised a new CyanoHAB delineation index named BWAI for the common spectral bands of Landsat and MODIS imagery by detecting the reflectance peak of green and NIR bands and modulating the peak regarding interferences from water suspended sediments in different scenarios.

#### 3.2.1. Detecting green or NIR reflectance peaks

We propose to detect green or NIR reflectance peaks of CyanoHABs by searching for the larger reflectance from green and NIR bands above a baseline determined by the blue and SWIR bands that are with shorter and longer wavelengths. The reflectance peaks at the green and NIR bands can account for subsurface algal blooms without scums in mesotrophic/eutrophic waters and floating scums/mats in hypertrophic waters, respectively. The green or NIR Reflectance Peak Height, i.e.,  $RPH_{(Green, NIR)}$ , of Landsat and MODIS imagery is calculated as:

$$RPH_{(Green, NIR)} = \rho_{max} - \rho_{blue} - (\rho_{SWIR} - \rho_{blue}) \times \frac{\lambda_{max} - \lambda_{blue}}{\lambda_{SWIR} - \lambda_{blue}} \quad (1)$$

where  $\rho_{max}$  represent the maximal water surface reflectance of the green and NIR bands, and  $\lambda_{max}$  is the corresponding central wavelength;  $\rho_{blue}$  and  $\rho_{SWIR}$  are the water surface reflectance of the blue and SWIR bands, respectively, and  $\lambda_{blue}$  and  $\lambda_{SWIR}$  are the correspondingly central wavelengths. Specifically, the central wavelengths of the involved bands are referred to Table 1.

#### 3.2.2. Depressing green or NIR reflectance peaks

For waters with high suspended sediment and low cyanobacteria loadings, e.g., muddy waters, the green or NIR reflectance peak caused by suspended sediment reflection needs to be depressed to avoid false positives. The red band of Landsat is not only strongly absorbed by chlorophyll in CyanoHABs but also significantly reflected by suspended sediments (Vincent et al., 2004), which has the maximum sensitivity to suspended sediment concentration and can be used to discriminate waters with different turbidity levels (Mertes et al., 1993). For instance, Kahru et al. (2007) utilized a threshold method based on the MODIS red band to build a water turbidity flag to remove high turbidity pixels that may lead to false positives. Since single band threshold methods

or band ratios are sensitive to image noises and atmospheric correction uncertainties, we designed a robust depressing factor based on red reflectance peak heights to extract high turbidity pixels and depress the corresponding green or NIR reflectance peak:

$$F_S = \exp(\rho_{\text{Red}} - \rho_{\text{Green}} - (\rho_{\text{NIR}} - \rho_{\text{Green}}) \times \frac{\lambda_{\text{Red}} - \lambda_{\text{Green}}}{\lambda_{\text{NIR}} - \lambda_{\text{Green}}}) \quad (2)$$

where  $\rho_{\text{Green}}$ ,  $\rho_{\text{Red}}$ ,  $\rho_{\text{NIR}}$  and  $\lambda_{\text{Red}}$ ,  $\lambda_{\text{Green}}$ ,  $\lambda_{\text{NIR}}$  represent the water surface reflectance and central wavelengths of the green, red, and NIR bands. Specifically, the central wavelengths of the involved bands are referred to Table 1. Pixels with positive red peak heights will be regarded as high turbidity waters, and  $RPH_{(\text{Green}, \text{NIR})}$  will be depressed by dividing  $F_S$ .

### 3.2.3. Modulating green or NIR reflectance peaks

For waters with CyanoHABs and relatively low suspended sediment loadings, the red band still appears as absorption characteristics due to the absorption effects of water and CyanoHABs, thereby leading to zero or negative red reflectance heights. Therefore, the green or NIR reflectance peak needs to be modulated further. Pure waters have higher reflectance at blue bands than the other bands due to the less water absorption at blue bands (Kutser, 2009), but waters with CyanoHABs have low and high water-leaving reflectance at blue and green bands due to the extra absorption and reflectance from chlorophyll (Gitelson, 1993; Gower, 1980), which enables chlorophyll concentration estimation by green to blue ratios (Gower, 1980). However, water suspended sediments increase the reflectance of blue bands significantly (Ritchie et al., 1976), thereby leading to higher blue reflectance than pure waters. That is, suspended sediments enhance the blue reflectance significantly while CyanoHABs do not. Hence, we use a signal modulation factor based on the normalized difference ratio of blue and green bands to modulate the green or NIR reflectance peak:

$$F_C = \exp((\rho_{\text{Green}} - \rho_{\text{Blue}})/(\rho_{\text{Green}} + \rho_{\text{Blue}})) \quad (3)$$

where  $\rho_{\text{Green}}$  and  $\rho_{\text{Blue}}$  represent the water surface reflectance at the green and blue bands. The normalization by the sum of green and blue reflectance can eliminate observation differences and uncertainties in estimating water surface reflectance (Mishra and Mishra, 2012), which is more robust than calculating band ratios of green to blue directly (Gower, 1980). Although suspended sediments increase the green reflectance as well, the  $F_C$  of CyanoHAB affected waters has higher magnitudes than the  $F_C$  of suspended sediment affected waters because of the absorption and reflection effects on blue bands caused by CyanoHABs and suspended sediments, respectively. Therefore, multiplying  $F_C$  with  $RPH_{(\text{Green}, \text{NIR})}$  can further enhance the green or NIR reflectance peak of CyanoHABs, thereby leading to weaker reflectance heights for waters affected by suspended sediments.

Based on Eqs. (1)–(3), the modulated green or NIR reflectance peak height for Landsat and MODIS imagery, i.e., BWAI, can be calculated:

$$\text{BWAI} = RPH_{(\text{Green}, \text{NIR})} \times \begin{cases} F_C, & \ln(F_S) \leq T \\ F_S^{-1}, & \ln(F_S) > T \end{cases} \quad (4)$$

where  $T$  is a threshold to extract high turbidity waters. The recommended range of  $T$  is -0.015 - 0.003 in practice due to remote sensing image noises or uncertainties in atmospheric corrections, and 0.003 was adopted in this study. Consequently, algal bloom index images with complementary spatial and temporal resolutions derived from Landsat and MODIS observations can be obtained, which provide fine-but-sparse and coarse-but-frequent data sources for the following spatial-temporal image fusion process to generate fine-and-frequent BWAI images.

### 3.3. Blending Landsat- and MODIS- derived CyanoHAB indices

STIF utilizes prior coarse- and fine- resolution image pairs on base dates and coarse-resolution images on prediction dates to predict fine-resolution images on prediction dates (Huang and Zhao, 2017). The involvement of STIF is to fuse the fine-but-sparse Landsat and coarse-but-frequent MODIS BWAI images to generate fine-and-frequent Landsat-like BWAI image series that have the spatial resolution of Landsat and

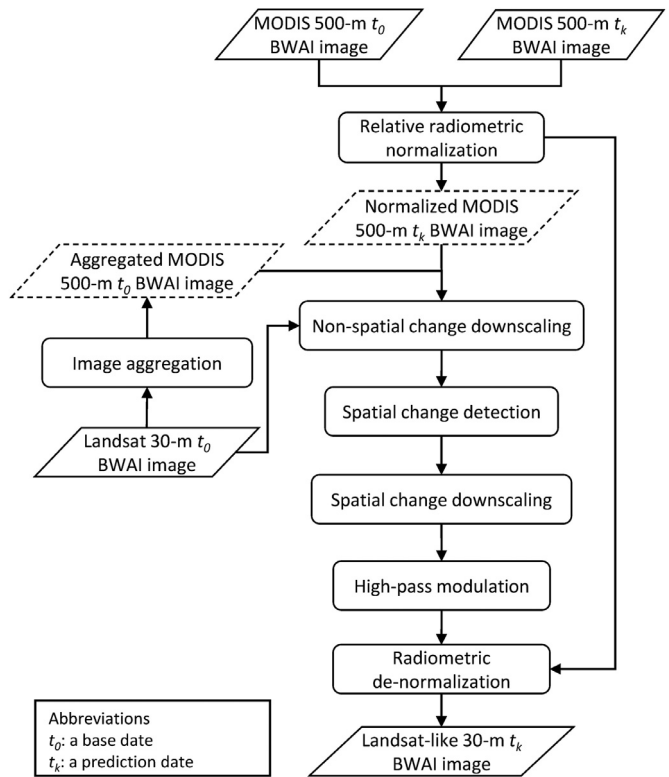


Fig. 3. The RASTFM flow chart for the spatiotemporal fusion of BWAI imagery.

the temporal resolution of MODIS. The STIF is conducted based on BWAI indices directly rather than individual image bands because an index-then-blend approach is suggested for water environmental index fusion due to: (1) higher fusion accuracy owing to less error propagation, (2) less computational burden because of fusion to single band indices rather than multiple image bands, and (3) lower sensitivity to fusion algorithm choice (Jarihani et al., 2014).

Considering the fast-changing dynamics and patchy characteristics of spatial distributions of CyanoHABs (Yacobi et al., 1995), part of temporal changes of algal blooms are spatial changes regarding their changes in the spatial domain (especially for floating scums with extremely high algal biomass), and the spectral changes of subsurface blooms or waters can be regarded as non-spatial changes. Hence, RASTFM (Zhao et al., 2018b) is employed for STIF because it can handle both non-spatial and spatial changes with outstanding performances by the combination of a non-spatial change downscaling module and a spatial change downscaling module that are both based on the non-local linear regression theory (Zhao et al. 2018b). Moreover, unlike other STIF methods that require two prior coarse- and fine- resolution image pairs on two base dates (Huang and Zhang, 2014; Zhu et al., 2010), RASTFM requires only one prior coarse- and fine- resolution image pair on a base date. The requirement of less fine-resolution prior images is important for this research because there are very few cloud-free Landsat-8 images over the whole western Lake Erie during its CyanoHAB season (relatively more precipitation leads to more cloudy weather). For instance, only the Landsat-8 image on September 26, 2017 is cloud-free for western Lake Erie from August to October. The flow chart of RASTFM for the spatiotemporal fusion of BWAI imagery is shown in Fig. 3. For more details about RASTFM, we refer readers to (Zhao et al., 2018b).

### 3.4. Validation

#### 3.4.1. CyanoHAB index development

We compared the proposed BWAI method with the representative algal bloom delineation algorithms that are also based on satellite imagery

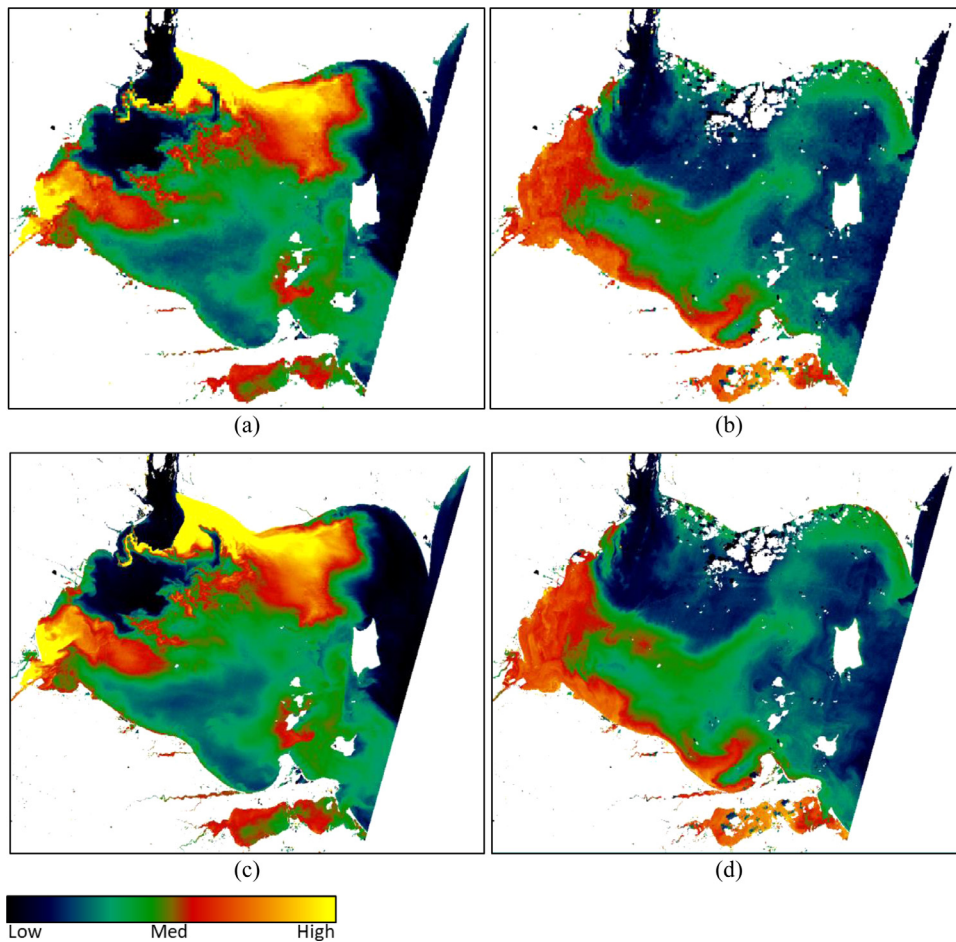


**Fig. 4.** The STIF for CyanoHABs mainly with subsurface blooms. The (a, c) and (b, d) are the MODIS-Landsat image pairs on September 26 and August 25 in 2017, respectively.

with a few broad wavelength bands, i.e., Landsat, including NIR to red ratio (N/R; [Yacobi et al., 1995](#)), NIR to green ratio (N/G; [Gitelson et al., 1993](#)), red to green ratio (R/G; [Gitelson et al., 1993](#)), (blue – red) to green ratio ((B-R)/G; [Mayo et al., 1995](#)), Improved NIR with Simple Atmospheric Correction (INSAC; [Ho et al., 2017](#)), and FAI ([Hu, 2009](#)). Visual comparisons of Landsat and MODIS derived algal indices and the reference cyanobacteria indices over western Lake Erie were performed to qualitatively evaluate the indicative effects of these methods regarding the spatial distributions and magnitudes of CyanoHABs. Quantitatively, natural logarithmic transformed *in situ* PC and Chl-a concentrations from the 12 buoys on the 16 dates in [Table A1](#) of the Appendix are fitted with the corresponding log-transformed algae index values by linear regressions to examine their correlations regarding Pearson correlation coefficients (R), scatter plots, and the fitted significance in terms of *P*-values. A  $3 \times 3$  window was used to extract pixel values and then averaged for each buoy to reduce sensor noises ([Lathrop, 1992](#); [Mayo et al., 1995](#)). The natural logarithmic transformation is to obtain the highest correlation ([Gitelson et al., 1993](#)).

#### 3.4.2. CyanoHAB index fusion

To examine the downscaling effects of the RASTFM based STIF in different CyanoHAB scenarios, we conducted two STIF experiments regarding the algal blooms that were with few and significant floating scums, respectively (see [Figs. 4 and 5](#)). The two reference Landsat-8 OLI images were acquired on August 25, 2017 and July 30, 2019, which are with relatively less cloud coverage. The Landsat input for STIF on the base date was selected as the observation on September 26, 2017 because it is a Landsat-8 observation that is cloud-free over the entire western Lake Erie during the CyanoHAB season of western Lake Erie. Note

that the 500-m MODIS inputs for STIF were obtained by down-sampling their 30-m Landsat-8 counterparts. The reason why we adopted simulated MODIS rather than observed MODIS was to exclude the radiometric and geometric inconsistency caused by sensor and observing condition differences, then evaluating STIF performances by highlighting the prediction errors from the fusion algorithm itself explicitly ([Gevaert and García-Haro, 2015](#)). Additionally, since there is a temporal gap (about 3 h) between the Landsat and MODIS imaging time, CyanoHABs captured by Landsat and MODIS observations on the same day could be inconsistent due to the fast-changing characteristics of CyanoHABs. This issue can also be excluded by using simulated MODIS images.

The qualitative evaluations of STIF were conducted by comparing fused Landsat-like and true Landsat BWAI images to examine the fusion accuracy regarding their spectral fidelity, structural similarity, etc. In addition, visual inspections were also performed to examine the sharpness enhancement effects of the fused fine-resolution Landsat-like BWAI images over their coarse-resolution MODIS counterparts. Quantitative metrics were calculated between fused and true fine-resolution BWAI images from image spectral and structure similarity perspectives. The R, Root Mean Square Error (RMSE), and Average Absolute Difference (AAD) between fused Landsat-like and true Landsat images were used to evaluate the spectral similarity; the Structural SIMilarity (SSIM) index ([Wang et al., 2004](#)) values were adopted to assess the structural similarity. Additionally, the absolute difference maps between fused and reference BWAI images were used to demonstrate the spatial distributions and magnitudes of fusion errors. The scatter plots between the fusion and reference values provided an intuitive comparison in describing the approximate extent of the distribution regarding their correlation ([Zhao et al., 2018b](#)).

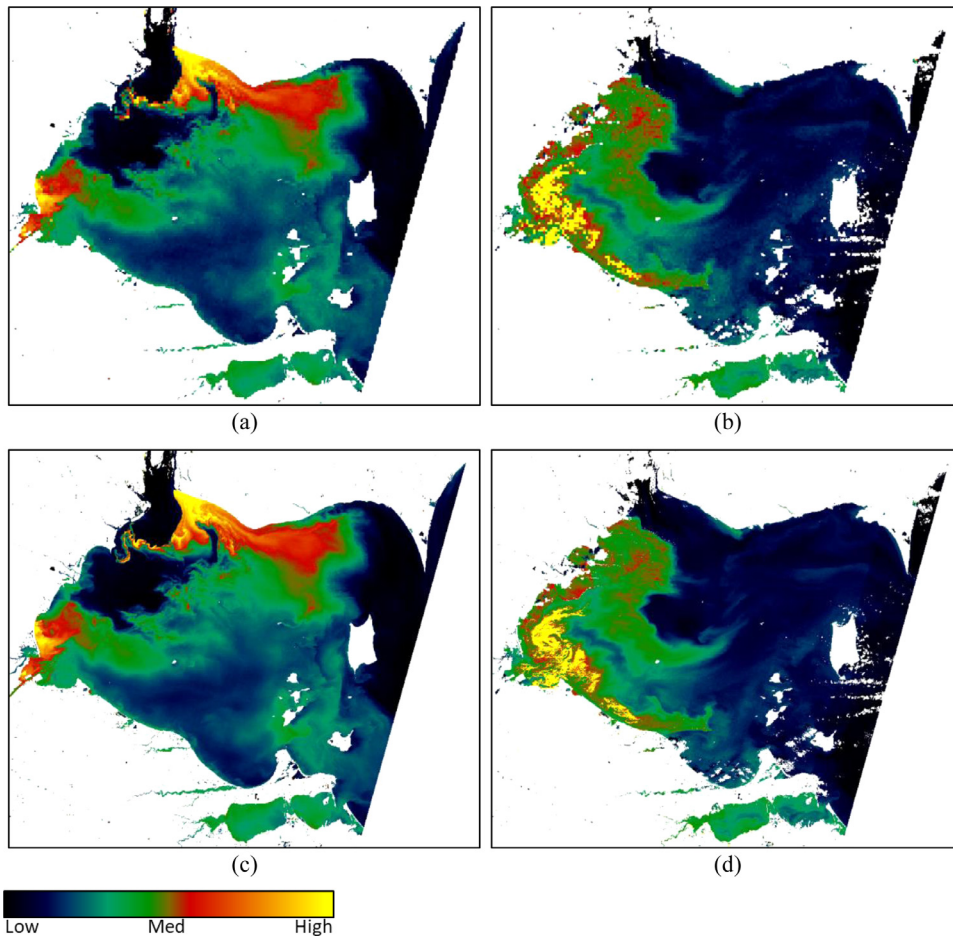


**Fig. 5.** The STIF for CyanoHABs with both subsurface blooms and floating scums. The (a, c) and (b, d) are the MODIS-Landsat image pairs on September 26, 2017 and July 30, 2019, respectively.

To complement the simulation tests to evaluate the downscaling contribution of STIF, we predicted the Landsat-like BWAI images on the 16 dates in [Table A1](#) of the Appendix based on the actual MODIS BWAI images rather than the simulated one. Then, the synchronous *in situ* CyanoHAB pigment concentrations extracted from the real-time observations, i.e., PC and Chl-a, on these dates were correlated with the fused fine-resolution Landsat-like BWAI values in terms of Rs and scatter plots to examine whether the STIF process improved the correlations comparing with the results based on the coarse-resolution MODIS BWAI values.

The evaluation criteria for the STIF process were: (1) the closer R and SSIM were to one, the more similar the predictions were to the references; (2) the closer RMSE, AAD, and absolute difference map were to zero, the more similar the predictions were to the references; (3) the closer the scatter plots were to the 1:1 line, the more similar the predictions were to the references.

#### 4. Experimental results

##### 4.1. Landsat- and MODIS- derived CyanoHAB indices

###### 4.1.1. Landsat-derived CyanoHAB indices

For representative CyanoHABs with few and significant floating scums, we selected the Landsat-8 OLI observations of western Lake Erie on September 26, 2017 and July 30, 2019, respectively. Then, we compared the newly developed CyanoHAB index, i.e., BWAI, with the comparative algae indices derived from the two OLI observations (see [Figs. 6 and 7](#)). The corresponding CI images ([Wynne et al., 2008](#)) derived from the 1000-m Aqua MODIS and 300-m Sentinel-3 OLCI bands ([NOAA, 2019](#)) were adopted as references for the spatial distributions and magnitudes of the CyanoHABs (see [Figs. 6a and 7a](#)). Furthermore,

the true-color and false-color images are used to demonstrate the spectral features of the CyanoHABs (see [Figs. 6b-c and 7b-c](#)). The waters with green patches in [Figs. 6b](#) and [7b](#) represent the CyanoHABs, and the depth of the green color is proportional to the biomass of the blue-green algae, which demonstrate the effectiveness of the green band. Moreover, there are few red patches on the water surface regarding the false-color image in [Fig. 6c](#), which means few surface scums were formed on September 26, 2017 because red patches represent extremely high reflectance at NIR bands caused by floating scums. However, there are some red patches in the southwest of western Lake Erie regarding the false-color image in [Fig. 7c](#), indicating patchy surface scums were formed by CyanoHABs on July 30, 2019.

For the overall qualitative comparisons regarding the spatial distributions and magnitudes of the CyanoHABs with few floating scums in [Fig. 6](#), the R/G, INSAC, and proposed BWAI images have consistent trends with the CI image; the (B-R)/G and FAI images have opposite trends with the CI image; the N/R and N/G images have low visual similarities with the CI image. However, since high FAI values represent algal blooms with high biomass, the CyanoHAB distributions in the FAI image are inconsistent with the actual spatial patterns of the CyanoHABs. For the visual evaluations of the CyanoHABs with significant floating scums in [Fig. 7](#), the N/R, N/G, INSAC, and FAI images are indicative regarding the floating scums but less indicative regarding the subsurface blooms; the R/G image shows low visual similarities with the CI image; the (B-R)/G image is with negative trends with the CI image; the proposed BWAI image has the highest visual similarity with the reference CI image.

Quantitatively, the OLI derived algal index values were evaluated by the corresponding *in situ* PC and Chl-a concentrations on the 16 dates in [Table A1](#) of the Appendix to examine their correlations. As indicated in

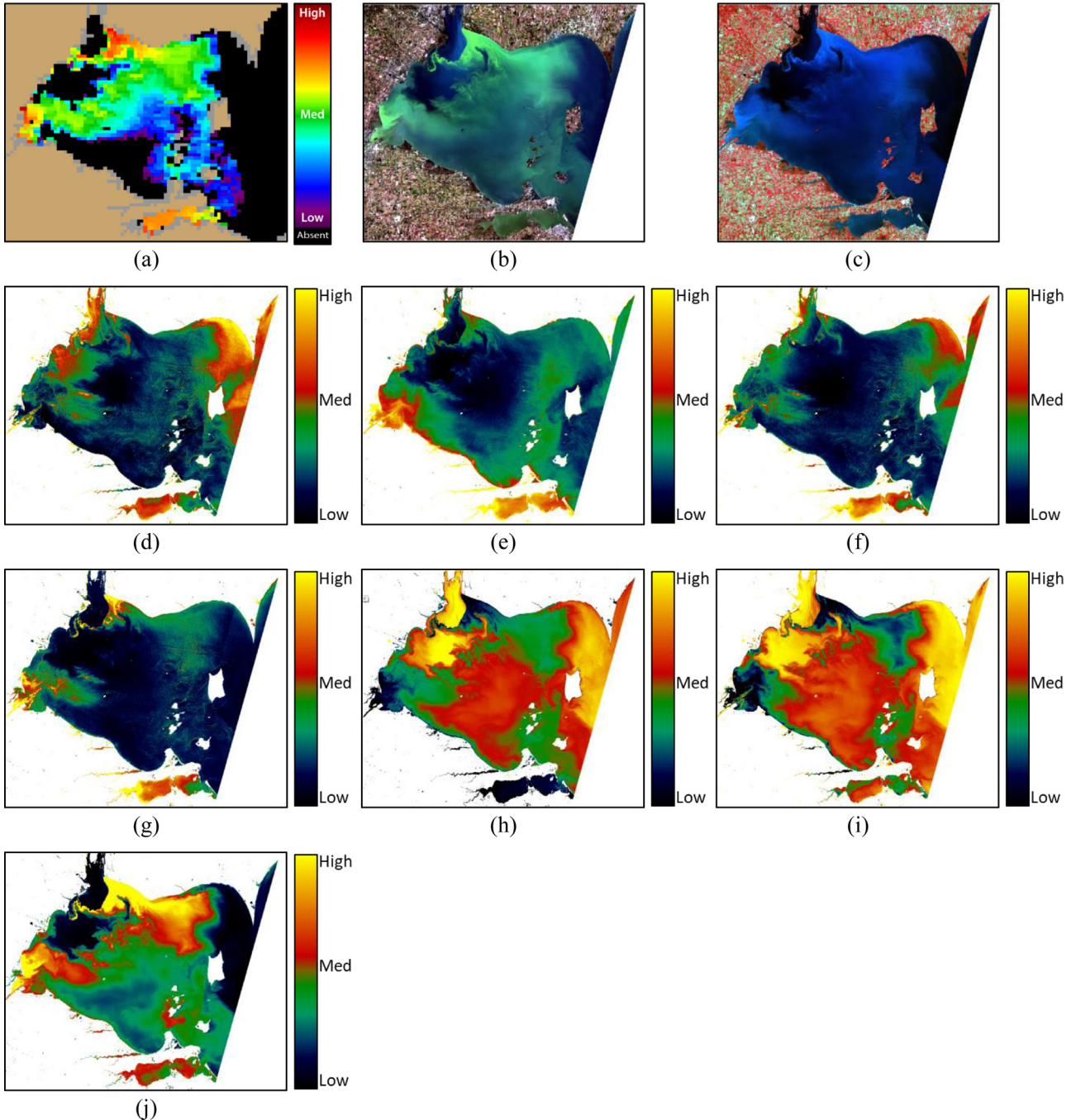


**Fig. 6.** The 1000-m Aqua MODIS CI image (NOAA 2019) of western Lake Erie on September 26, 2017 (a), and the corresponding 30-m Landsat-8 OLI true-color, false-color (NIR-red-green bands as R-G-B composites), N/R, R/G, N/G, INSAC, (B-R)/G, FAI, and propose d BWAI images (b)-(j). (For interpretation of the references to color in this figure legend, the reader is referred to the web version of this article.)

**Fig. 8**, the N/R values have the lowest correlation with *in situ* data (not significant with large  $P$  values), and the N/G, R/G, FAI values have comparable correlations with each other (a few of them are significant with  $P$  values less than 0.05), but relatively low. The (B-R)/G, INSAC, and proposed BWAI values are all very significant at the 0.0001 level. Additionally, the Landsat BWAI values ( $BWAI_L$ ) have the highest correlation with *in situ* PC and Chl-a concentrations compared to the other algae indices, which has the R values of 0.7466 and 0.7123, respectively.

#### 4.1.2. MODIS-derived CyanoHAB indices

For inter-sensor comparisons, the Aqua MODIS observations that are corresponding to the Landsat-8 observations on September 26, 2017 and

July 30, 2019 were adopted to illustrate inter-sensor differences, such as scale, spectral, and data quality differences. The MODIS based comparative algae indices and BWAI images are demonstrated in Figs. 9 and 10. For the CyanoHABs with few and significant floating scums, the N/R, R/G, N/G, and INSAC images have comparable visual similarities with the reference CI image; the similarities of the (B-R)/G, FAI, and proposed BWAI images to the CI image are similar with the previous visual evaluations for Landsat based indices. Note that the speckle noises and aliasing effects in some MODIS derived algae indices, e.g., the N/R images, are caused by the random inferior observations in certain MODIS bands.

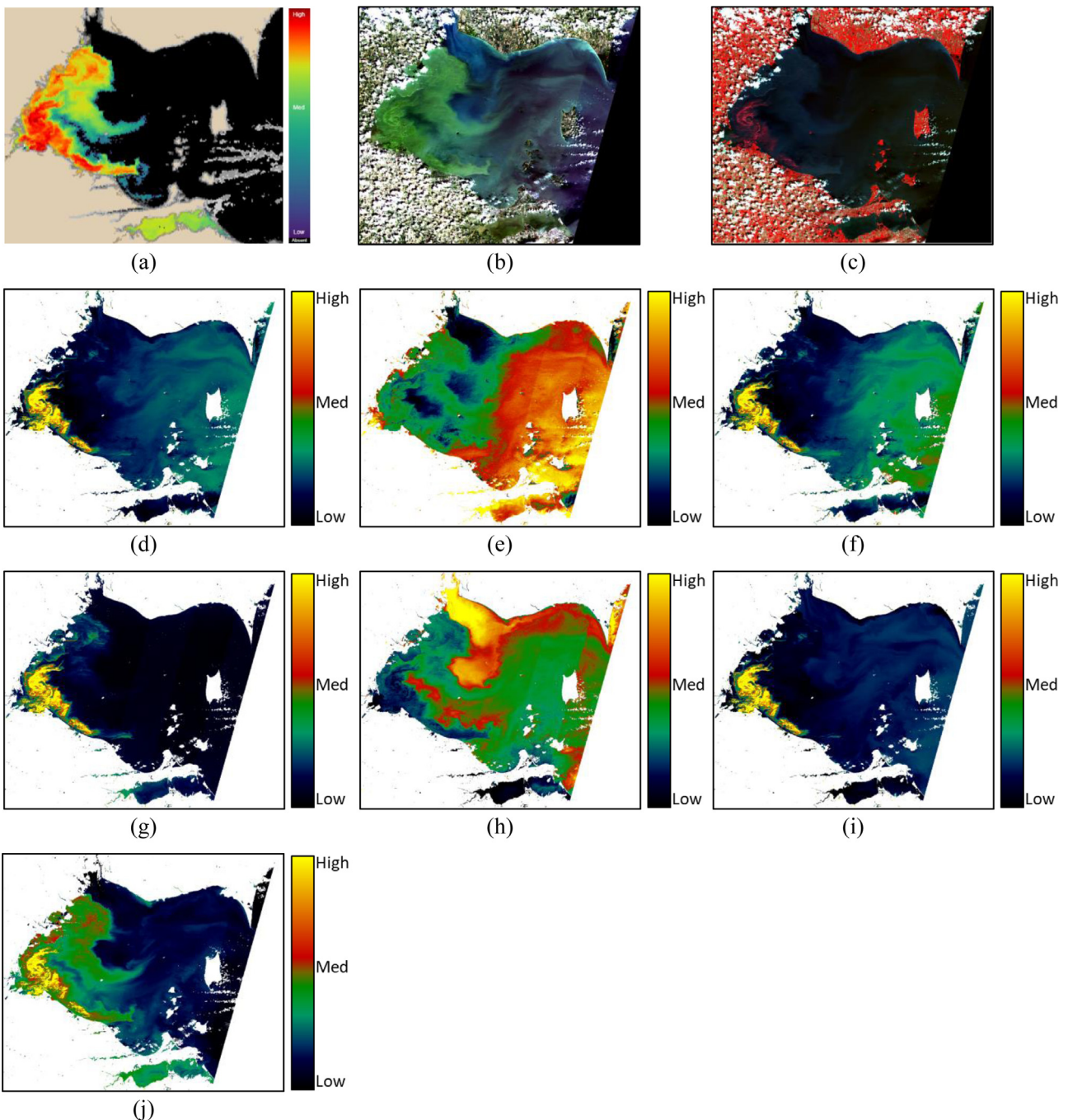


**Fig. 7.** The 300-m Sentinel-3 OLCI CI image (NOAA 2019) of western Lake Erie on July 30, 2019 (a), and the corresponding 30-m Landsat-8 OLI true-color, false-color (NIR-red-green bands as R-G-B composites), N/R, R/G, N/G, INSAC, (B-R)/G, FAI, and proposed BWAI images (b)-(j). (For interpretation of the references to color in this figure legend, the reader is referred to the web version of this article.)

Furthermore, the MODIS derived algae indices were correlated with the corresponding *in situ* CyanoHAB pigment concentrations, i.e., PC and Chl-a, for quantitative evaluations (see Fig. 11). It shows that the natural log-transformed MODIS BWAI values ( $BWAI_M$ ) have the highest correlations with the *in situ* observations, which are very significant at the 0.0001 level with the R values of 0.5406 and 0.5102. Note that the quantitative evaluations for MODIS- and Landsat- derived BWAI values were based on their common samples to highlight the fitting accuracy differences caused by the inter-sensor differences. It is obvious that the fine-resolution  $BWAI_L$  has higher correlations with *in situ* PC and Chl-a concentrations than the coarse-resolution  $BWAI_M$ . Since MODIS and Landsat BWAI images were derived by their common spectral bands, it

can be deduced that the inter-sensor differences of the fitting accuracy were mainly caused by the scale differences, i.e., 30-m versus 500-m spatial resolution. Given the better correlations of  $BWAI_L$  than  $BWAI_M$ , it is necessary and important to apply STIF to downscale coarse-resolution MODIS BWAI images to obtain fine-resolution Landsat-like BWAI images for dates without Landsat observations.

#### 4.2. Fused Landsat-like CyanoHAB indices

##### 4.2.1. STIF validation for fusing Landsat and MODIS BWAI

Qualitatively, the MODIS, true Landsat, and fused Landsat-like BWAI images on the prediction dates are presented for visual comparisons (see

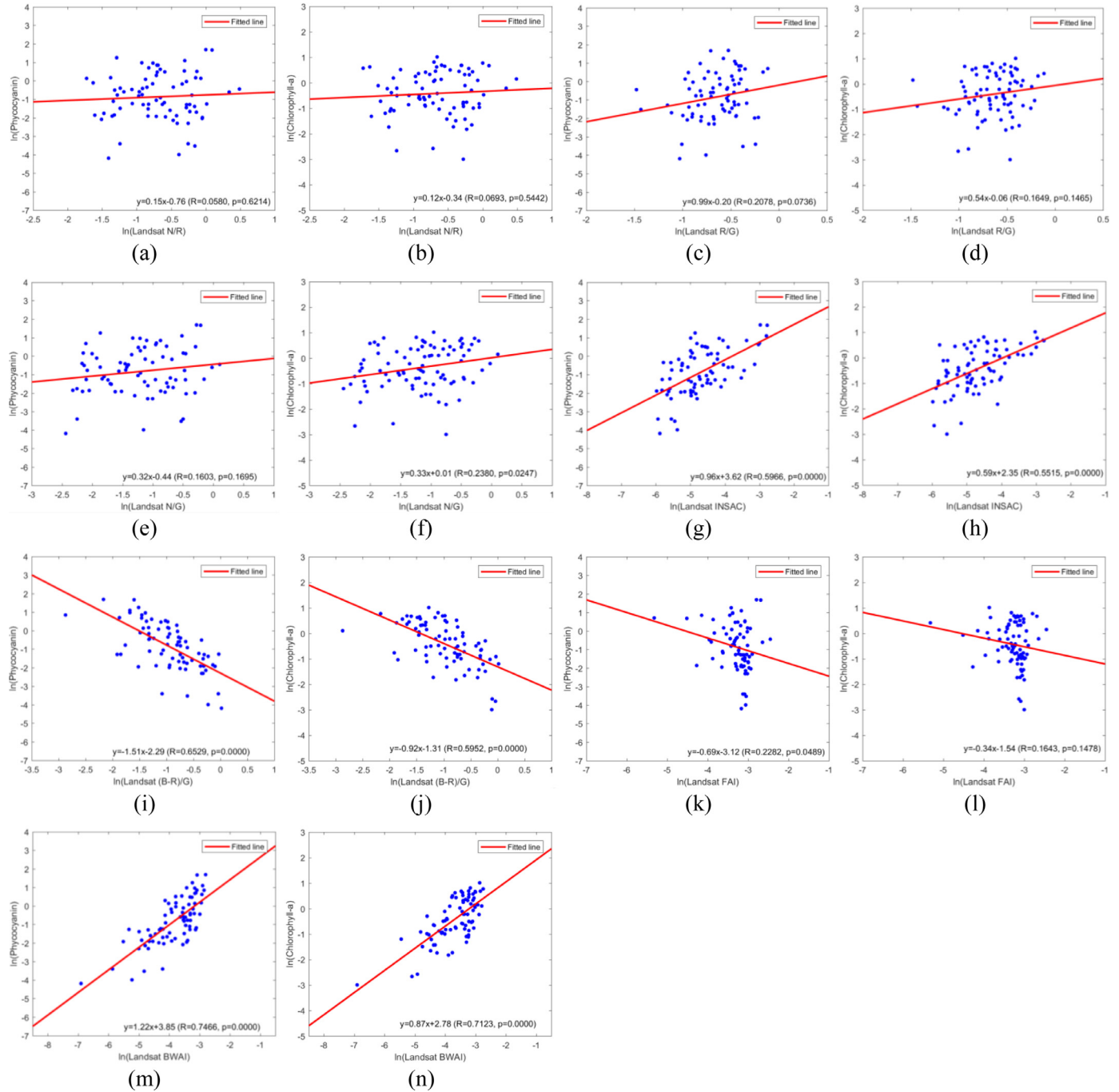


**Fig. 8.** The scatter plots between the 30-m Landsat log-transformed N/R, R/G, N/G, INSAC, (B-R)/G, FAI, and proposed BWAI values (X-axis) with the log-transformed *in situ* PC and Chl-a concentrations (Y-axis) on the 16 dates in Table A1 of the Appendix.

Figs. 12 and 13). Showing the prior MODIS BWAI image is to provide a benchmark to demonstrate the contribution of STIF regarding downscaling effects. It can be seen the fusion results (see Figs. 12c&f and 13c&f) not only show high visual similarities with the reference images (see Figs. 12a&d and 13a&d) but also have much more spatial details than the prior MODIS images (see the zoomed-in views in Figs. 12e&f and 13e&f).

Quantitatively, the absolute difference maps, scatter plots, and quantitative statistical metrics in Fig. 14 and Table 2 demonstrate that the fusion accuracy regarding the CyanoHABs with few floating scums is higher than the one regarding the CyanoHABs with significant floating scums. The reason is that the floating scums appearing on the prediction date are spatial changes, which are more difficult to be downscaled than

the non-spatial changes (Zhao et al., 2018b). However, the quantitative metrics indicate that the fusion results have very low biases and high similarities with the reference Landsat BWAI images. It means RASTFM downscales the coarse-resolution temporal change information from the prior MODIS images very well regarding spectral fidelity and image structure similarity. The reliable fusion accuracy of RASTFM proves its value for BWAI STIF and provides a solid foundation for downscaling MODIS BWAI image series.

#### 4.2.2. Batch STIF for high spatiotemporal resolution monitoring

To further evaluate the downscaling contribution of STIF quantitatively, the actual MODIS BWAI image series on the 16 dates in Table A1 of the Appendix were downscaled to 30-m via RASTFM to

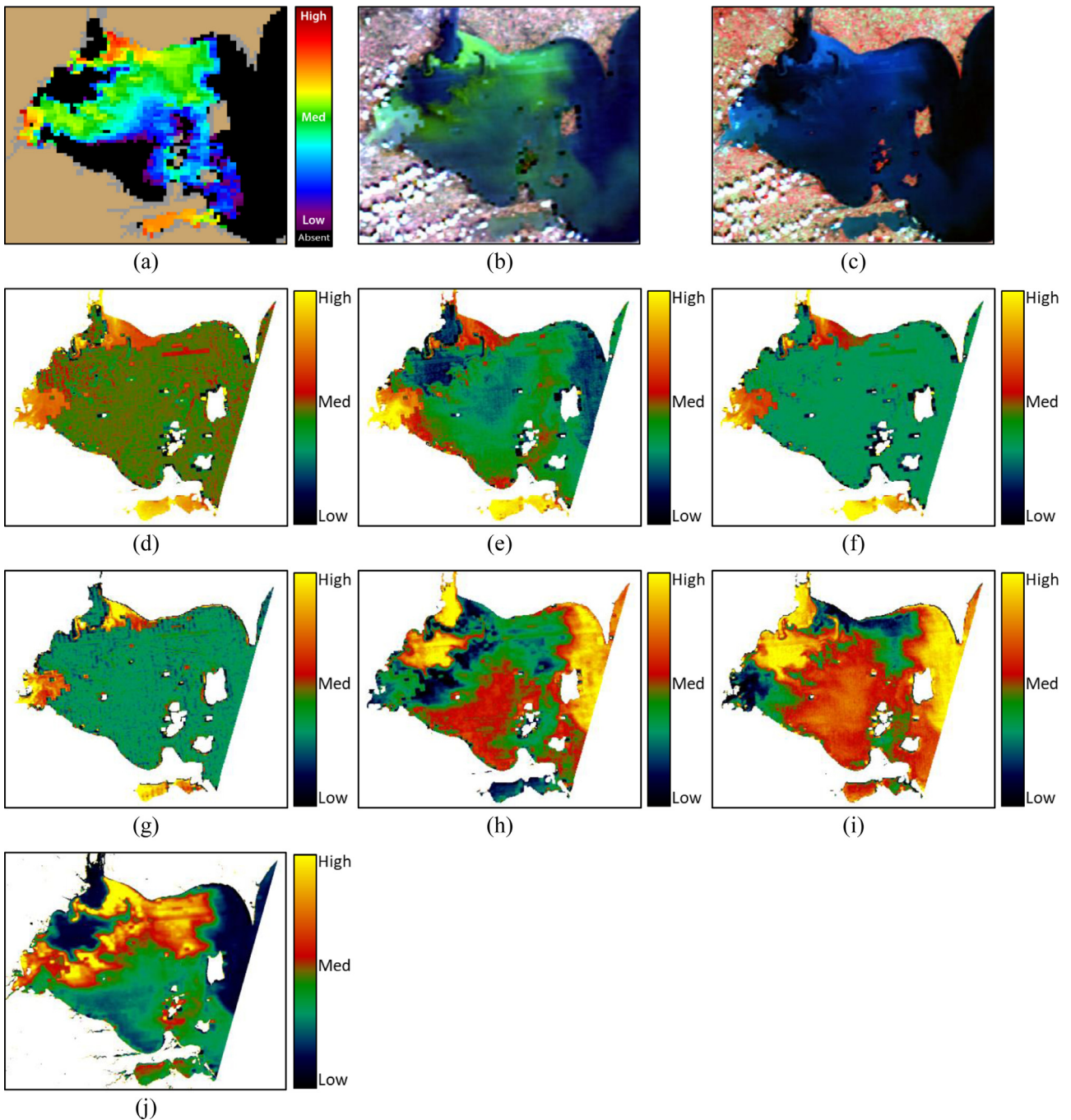


**Fig. 9.** The 1000-m Aqua MODIS CI image (NOAA 2019) of western Lake Erie on September 26, 2017 (a), and the corresponding 500-m MODIS true-color, false-color (NIR-red-green bands as R-G-B composites), N/R, R/G, N/G, INSAC, (B-R)/G, FAI, and proposed BWAI images (b)-(j). (For interpretation of the references to color in this figure legend, the reader is referred to the web version of this article.)

**Table 2**

The quantitative evaluation metrics of the fused Landsat-like BWAI images on August 25, 2017 (CyanoHABs with few floating scums) and July 30, 2019 (CyanoHABs with significant floating scums), respectively.

Image fusion scenario	R	RMSE	AAD	SSIM
CyanoHABs with few floating scums	0.9568	0.0033	0.0009	0.9616
CyanoHABs with significant floating scums	0.9305	0.0094	0.0022	0.9397

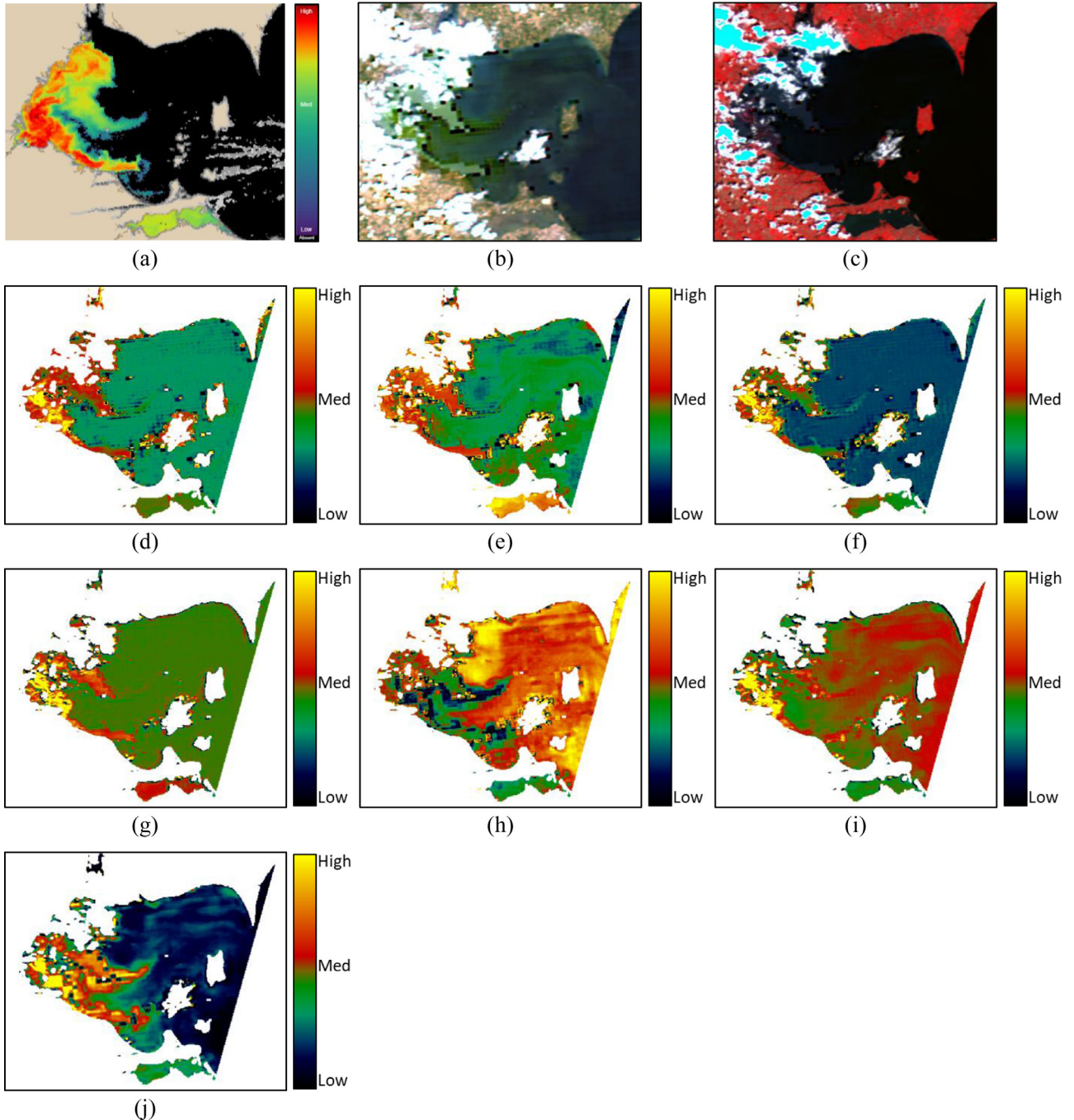


**Fig. 10.** The 300-m Sentinel-3 OLCI CI image (NOAA 2019) of western Lake Erie on July 30, 2019 (a), and the corresponding 500-m MODIS true-color, false-color (NIR-red-green bands as R-G-B composites), N/R, R/G, N/G, INSAC, (B-R)/G, FAI, and proposed BWAI images (b)-(j). (For interpretation of the references to color in this figure legend, the reader is referred to the web version of this article.)

generate their Landsat-like counterparts. Then, the natural logarithmic transformed *in situ* PC and Chl-a concentrations of the 12 sites and the corresponding log-transformed Landsat-like BWAI values ( $BWAI_L$ ) were fitted by linear regressions. The natural logarithmic transformation was to obtain the highest correlation (Gitelson et al., 1993). Additionally, the fitted results of  $BWAI_L$  and  $BWAI_M$  were presented to highlight the inter-sensor differences, and the fittings were based on the common data samples of  $BWAI_L$ ,  $BWAI_L$ , and  $BWAI_M$  to highlight their scale differences (see Fig. 15). It shows that all the three types of indices have very significant correlations with *in situ* CyanoHAB pigment concentra-

tions ( $P = 0.0000$ ).  $BWAI_L$  values have the highest correlation with *in situ* observations because they are true Landsat observations with 30-m resolution and high data quality. Since  $BWAI_L$  was downsampled from  $BWAI_M$ , their scatter plots are similar to a certain degree. However, the fine-resolution  $BWAI_L$  is more correlated with the *in situ* data than the coarse-resolution  $BWAI_M$ , indicating by their  $R_s$  of 0.6432 ( $BWAI_L$ -PC), 0.6110 ( $BWAI_L$ -Chl-a), 0.5406 ( $BWAI_M$ -PC), and 0.5102 ( $BWAI_M$ -Chl-a), respectively. Since STIF downscale changes information with coarse-resolution by adding spatial information, the only differences between  $BWAI_L$  and  $BWAI_M$  are their spatial resolutions, i.e., 30-m versus 500-

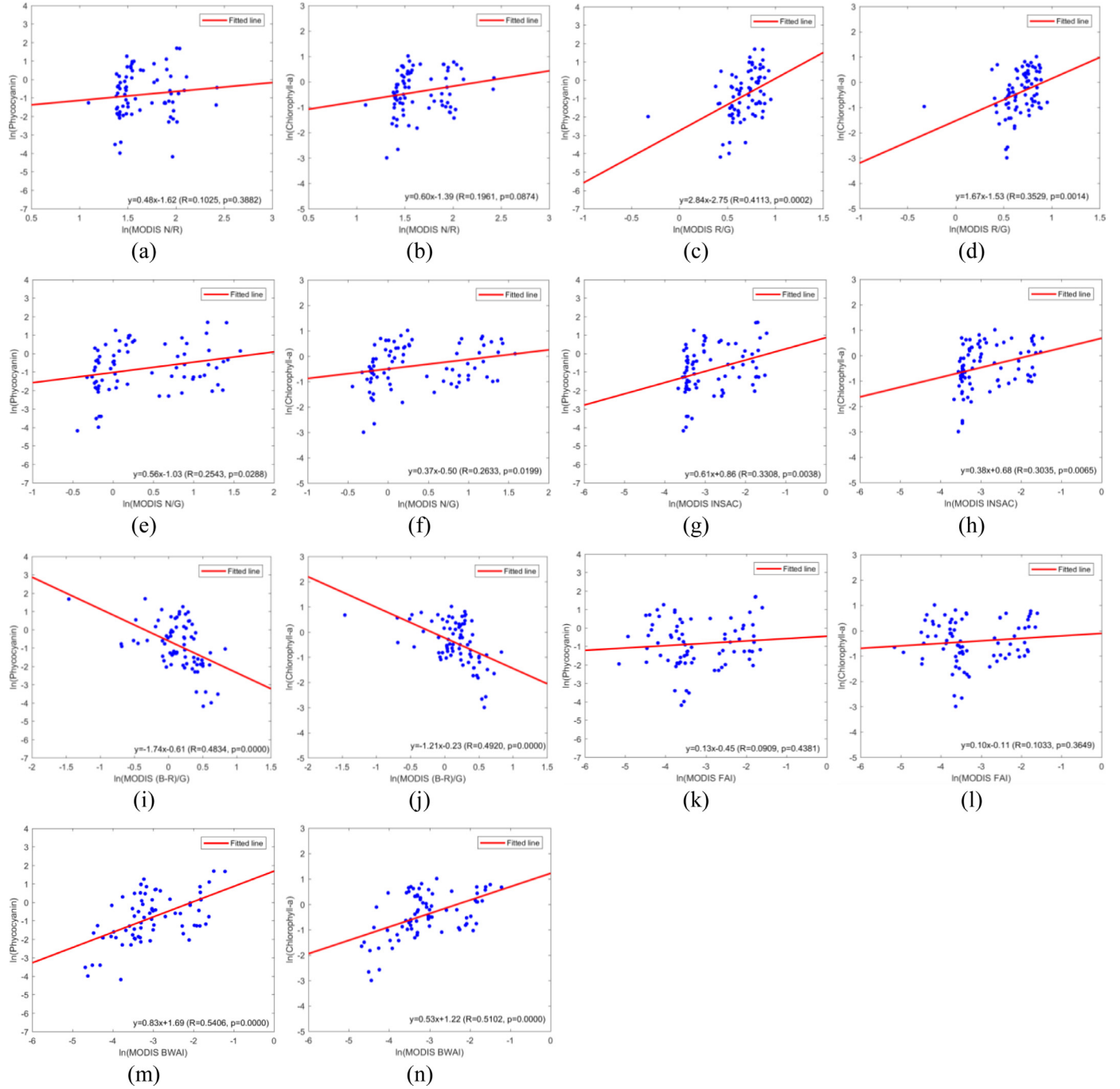


**Fig. 11.** The scatter plots between the log-transformed 500-m MODIS N/R, R/G, N/G, INSAC, (B-R)/G, FAI, and proposed BWAI values (X-axis) with the log-transformed *in situ* PC and Chl-a concentrations (Y-axis) on the 16 dates in Table A1 of the Appendix.

m. The higher fitting accuracy of BWAI<sub>L</sub> than BWAI<sub>M</sub> explicitly reveal the downscaling effects benefited from the RASTFM based STIF.

## 5. Discussion

In order to monitor CyanoHABs in western Lake Erie at high spatiotemporal resolution via STIF, a robust and indicative CyanoHAB spectral index that can be applied to both fine-but-sparse, e.g., Landsat, and coarse-but-frequent, e.g., MODIS, satellite imagery is needed. For the commonly used broad wavelength bands of Landsat for algae index derivation (e.g., blue, green, red, and NIR bands), blue, green, and red bands are prone to be affected by suspended sediments besides wa-

ter algae, which may introduce significant errors or false positives to algae indices. Therefore, algae indices that adopt these bands but do not consider the influence of suspended sediments would be less indicative, such as the comparative band ratio methods in Section 4.1. Although NIR bands are relatively less sensitive to suspended sediments than the visible bands (Nechad et al., 2010), the strong absorption from waters would reduce the reflectance of CyanoHABs significantly, especially for subsurface algal blooms with low/medium biomass. For instance, the method based on NIR reflectance peak heights, i.e., FAI, is indicative when CyanoHABs form floating scums/mats on water surface (usually with high algal biomass) but not indicative when they are beneath water surface due to relatively low biomass (Gower et al.,

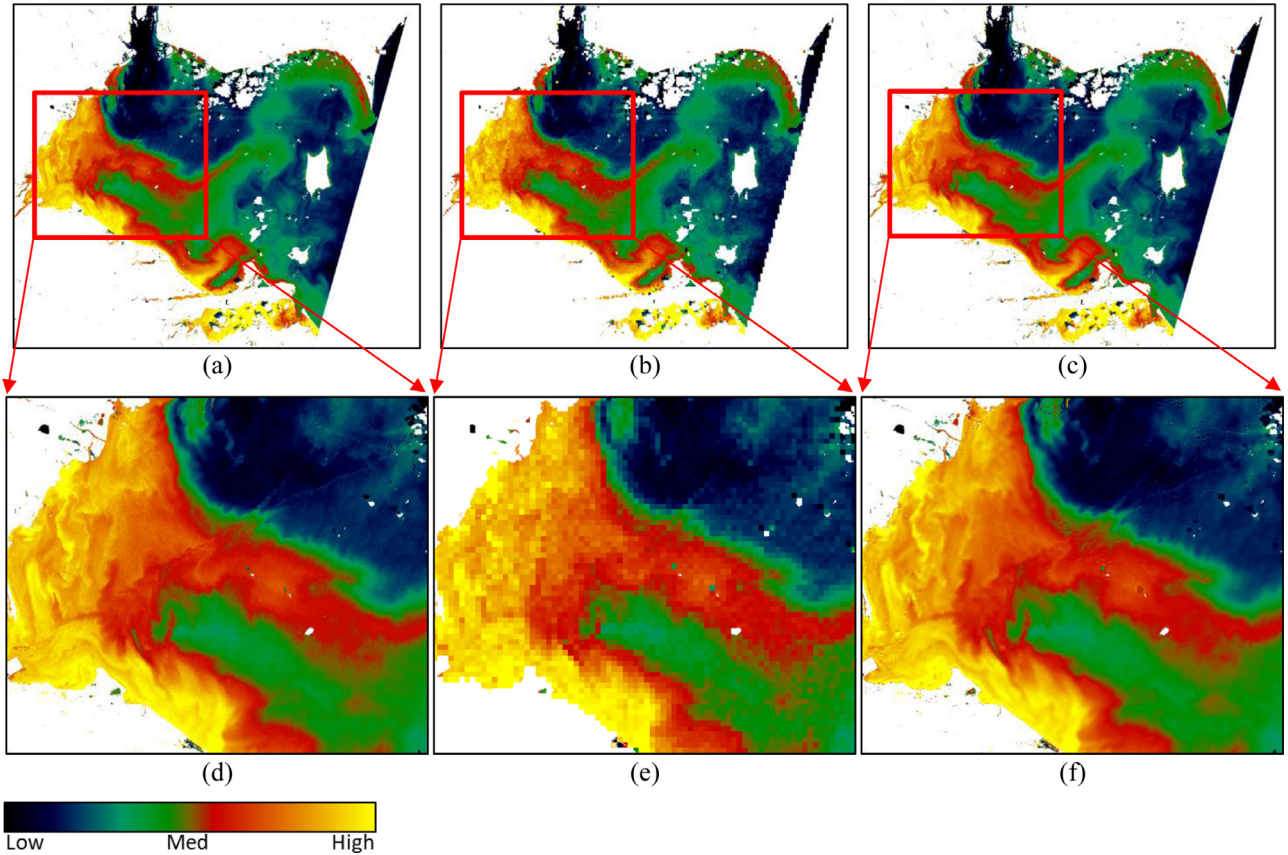


**Fig. 12.** Visual comparisons between the reference Landsat (a, d), MODIS (b, e), and Landsat-like BWAI images (c, f) on August 25, 2017 (CyanoHABs with few floating scums) as well as their local zoomed-in comparisons.

2005) or winds/waves mixing (Reutter, 2014). In our experiments, many CyanoHABs in western Lake Erie did not form floating scums but suspended beneath water surface, hence, FAI could not delineate the CyanoHABs accurately due to the few/weak reflectance peaks at NIR bands.

Given the deficiencies of the comparative algae indices in delineating the CyanoHABs in western Lake Erie with different biomass at multiple eutrophication levels, a CyanoHAB spectral index (BWAI) is developed based on the five common bands of Landsat and MODIS including the blue, green, red, NIR, and SWIR1 bands to mitigate the gaps mentioned above. First, BWAI calculates the larger reflectance peak height of the green and NIR bands, i.e.,  $RPH_{(\text{Green}, \text{NIR})}$ , which can account for subsurface algal blooms without scums in eutrophic waters and floating scums/mats formed by CyanoHABs in hypertrophic waters, respectively. Then, BWAI utilizes the depressing factor, i.e.,  $F_s$ , based on the red band reflectance height to depress the green or NIR peak regarding suspended sediment dominated waters to avoid large false positives caused by water suspended sediments. Additionally, BWAI uses the signal modulation factor, i.e.,  $F_c$ , based on the normalized difference ratio of green and blue bands to modulate the green or NIR peak for mixed waters with both CyanoHABs and low/medium suspended sediment loadings. For waters with other water constituents such as Chromophoric Dissolved Organic Matters (CDOM), the absorption of CDOM to short wavelength bands, e.g., the blue and green bands, may affect  $F_c$ , but the influence is at an acceptable level because both the blue and green bands would have absorption effects (Twardowski et al., 2004). Furthermore, the three components of BWAI, i.e.,  $RPH_{(\text{Green}, \text{NIR})}$ ,  $F_c$ , and  $F_s$ , are obtained by baseline calculation and normalized difference ratio, which makes BWAI quite robust and insensitive to mild sun-glint and atmosphere effects due to the advantages of these two types of calculation in algae index derivation (Mishra and Mishra, 2012; Stumpf et al., 2016).

Additionally, the calculation of the green or NIR reflectance peaks, i.e.,  $RPH_{(\text{Green}, \text{NIR})}$ , is similar with MPH (Matthews et al., 2012) by searching for maximum reflectance from several feature bands, which is more effective than baseline methods that only use one fixed central band because the multiple feature bands can address CyanoHABs in different situations. Consequently, these strengths enable BWAI to obtain outstanding indicative effects for CyanoHABs compared to the other algal indices devised for broad wavelength satellites.

Moreover, BWAI has broader sensor applicability than the baseline-based CyanoHAB spectral indices that are devised for coarse-but-frequent satellites, e.g., the MERIS based MPH and CI, because BWAI can be applied to both coarse-but-frequent (MODIS) and fine-but-sparse (Landsat) satellites. Therefore, BWAI not only improves the delineation accuracy of CyanoHABs based on the most popular fine-resolution satellite imagery (Landsat) but also provides a foundation for the posterior STIF to overcome the inherent compromise between the spatial and temporal resolution of satellites for high spatiotemporal resolution monitoring of CyanoHABs.

STIF is an important technology that can further exploit the value of the existing satellite imagery in remote sensing applications and theoretical studies that require high spatiotemporal resolution monitoring ability (Gao et al., 2015). Moreover, MODIS observations have lower signal-to-noise ratio than Landsat-8 observations due to its coarse resolution and calibration degradation caused by the longer serving time (Lyapustin et al., 2014), the blending of MODIS and Landsat imagery can improve the quality of the original MODIS images by generating their Landsat-like counterparts. Apart from land surface reflectance related applications, STIF has been widely used for other remote sensing derived products with fast-changing characteristics, such as land surface temperature (Weng et al., 2014), evapotranspiration (Cammalleri et al., 2013), soil moisture (Jiang et al., 2019), aerosol optical depth (Zhang, 2015),

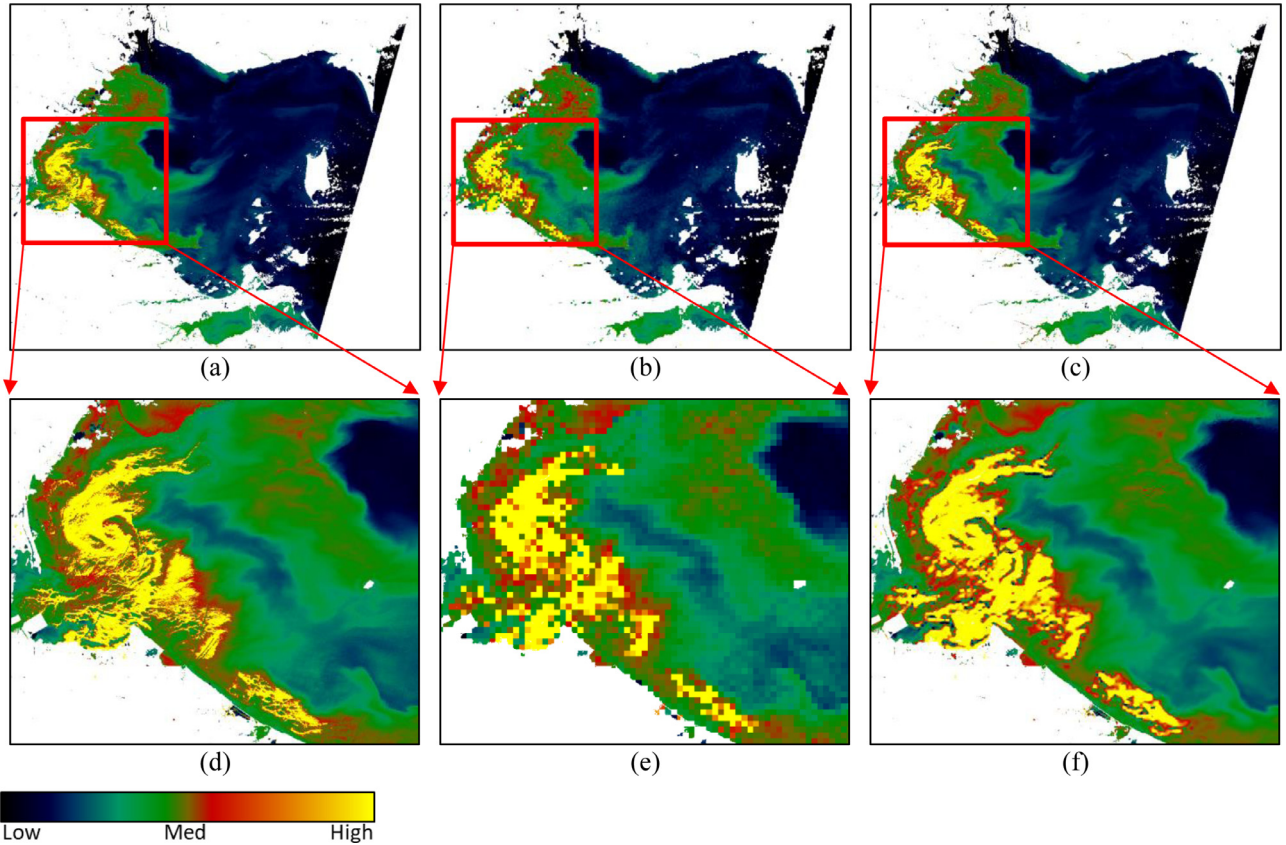


**Fig. 13.** Visual comparisons between the reference Landsat (a, d), MODIS (b, e), and Landsat-like BWAI images (c, f) on July 30, 2019 (CyanoHABs with significant floating scums) as well as their local zoomed-in comparisons.

air quality (Zhao et al., 2018a), and water quality (Swain and Sahoo, 2017). The life cycles and spatial distributions of CyanoHABs also change rapidly because they are driven by many fast-changing environmental factors, e.g., phosphorous concentration, water temperature, solar illumination, and hydrodynamics. MODIS and Landsat based BWAI images can capture temporal variations and spatial details of CyanoHABs, respectively, but they both have their pros and cons, i.e., coarse-but-frequent and fine-but-sparse. What is worse, cloud-free fine-resolution images would be much sparser during the CyanoHAB season than in other seasons, usually in summer, due to more cloudy and rainy weather conditions. Hence, STIF is necessary and applicable to blend their advantages to produce fine-and-frequent Landsat-like BWAI images for high spatiotemporal resolution monitoring.

Furthermore, CyanoHABs are with both non-spatial (e.g., subsurface blooms) and spatial changes (e.g., high algal biomass with surface scums) regarding the fast-changing dynamics and patchiness of the spatial distributions of CyanoHABs. For STIF, non-spatial changes mainly occur in the spectral domain rather than the spatial domain, while spatial changes have significant changes in the spatial domain (Zhao et al., 2018b). In this study, the subsurface blooms mainly have moderate changes in the spectral domain, and the CyanoHAB details do not change too much. However, the surface scums have significant changes in the spatial domain, thereby leading to many water surface details and severe spectral changes related to the CyanoHABs with high biomass (Kutser, 2004). Hence, RASTFM is adopted for BWAI STIF due to its outstanding performances in downscaling both non-spatial and spatial changes (Zhao et al., 2018b). The STIF results demonstrate that the fusion scenario of CyanoHAB changes with surface scums has lower fusion accuracy than the scenario mainly with subsurface blooms because spatial changes are more difficult to predict than non-spatial changes (Zhao et al., 2018b). More importantly, the Landsat-like BWAI

images have higher spatial resolutions than the MODIS BWAI images in terms of image sharpness. Moreover, the fine-resolution Landsat-like BWAI values have higher correlations with the *in situ* PC and Chl-a concentrations than their coarse-resolution MODIS counterparts. Note that the RASTFM based STIF provides us an alternative to obtaining fine-and-frequent BWAI image series, but it cannot replace actual Landsat observations.

While ENVISAT MERIS and Sentinel-3 OLCI can provide indicative CyanoHAB indices (such as CI and MPH) thanks to their ample spectral bands, they cannot resolve spatial details of CyanoHABs or delineate CyanoHABs in small water bodies because of their coarse spatial resolutions (300-m to 1200-m). Moreover, the data archive periods of MERIS (2002-2012) and OLCI (2016-present) are much shorter than Landsat (1984-present, starting from Landsat-5) and MODIS (1999-present). Additionally, both Landsat and MODIS have continuous observation plans to guarantee data consistency (Wulder et al., 2019; Zhou et al., 2019). These advantages of Landsat and MODIS are of crucial importance for the long-term and consistent investigation of CyanoHAB changes in western Lake Erie or global lakes (Ho et al., 2019). Therefore, this research adopts Landsat and MODIS imagery as fine-but-sparse and coarse-but-frequent data sources for CyanoHAB monitoring, and the posterior STIF approach further provides valuable results by blending the merits of the two data sources.

## 6. Conclusions

In conclusion, this study presents an effective and low-cost solution for high spatiotemporal resolution monitoring of CyanoHABs in western Lake Erie based on a novel spectral index, i.e., BWAI, and the RASTFM based STIF. Specifically, it blends BWAI images derived from fine-but-sparse (Landsat) and coarse-but-frequent (MODIS) satellite observations

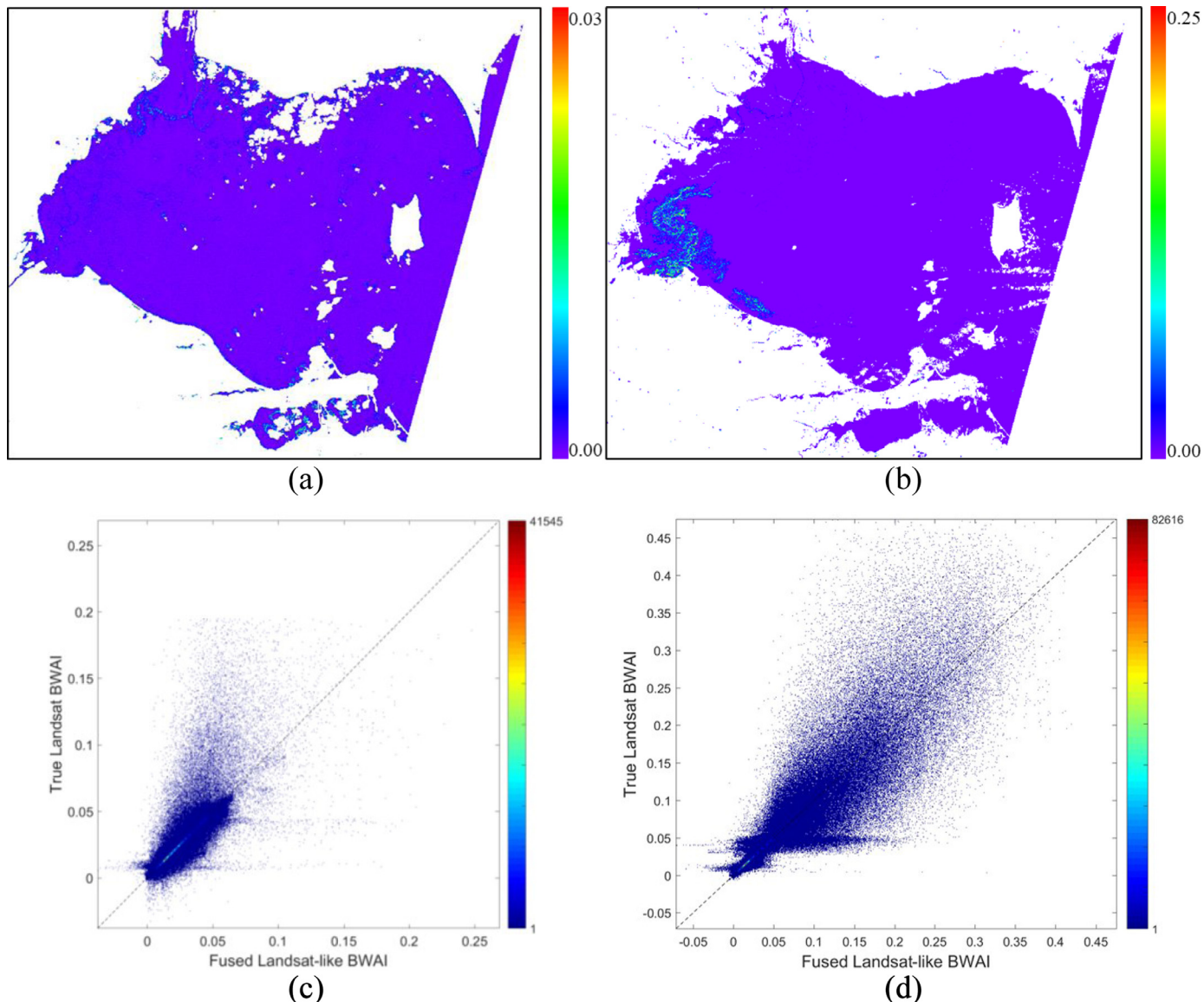


**Fig. 14.** The absolute difference maps and scatter plots between the reference Landsat and fused Landsat-like BWAI images on August 25, 2017 (a, c) and July 30, 2019 (b, d).

to generate fine-and-frequent Landsat-like BWAI image series for high spatiotemporal resolution monitoring of CyanoHABs. BWAI is more indicative to CyanoHABs than the comparative algal bloom indices because BWAI can delineate CyanoHABs with and without floating scums simultaneously and mitigate the interference of suspended sediments. STIF is a useful solution to the shortages of existing buoy- and satellite-based observation systems from a cost-effective “software” perspective rather than a costly “hardware” perspective to deploy more buoys or launch more satellites. Moreover, introducing STIF to CyanoHAB monitoring further promotes the application of STIF in remote sensing communities. This research is an important and significant supplement to existing CyanoHAB studies by achieving high spatiotemporal resolution monitoring, thereby quantifying their fine-resolution spatial-temporal variations.

In our future studies, fine-and-frequent CyanoHAB pigment (PC and Chl-a) maps of inland lakes will be accurately estimated by integrating fine-and-frequent BWAI image series and related water environmental parameters, e.g., water temperature, phosphorus, turbidity, via regression analysis or machine learning models. Practi-

cally, the outcomes will be useful in many ways, such as CyanoHAB studies and aquatic ecosystem evaluation for researchers, CyanoHAB treatment policy making for local authorities, loss reduction decision making for management agencies and private sectors, and cyanobacterial toxin-caused hazard resilience understanding for local communities.

#### Declaration of Competing Interest

None.

#### Acknowledgment

The authors would like to thank three anonymous reviewers for their comments and suggestions, which greatly helped to improve this manuscript. This study was supported by the United States Department of Agriculture under the [National Institute of Food and Agriculture Capacity Building Grant # 2017-38821-26419](#).

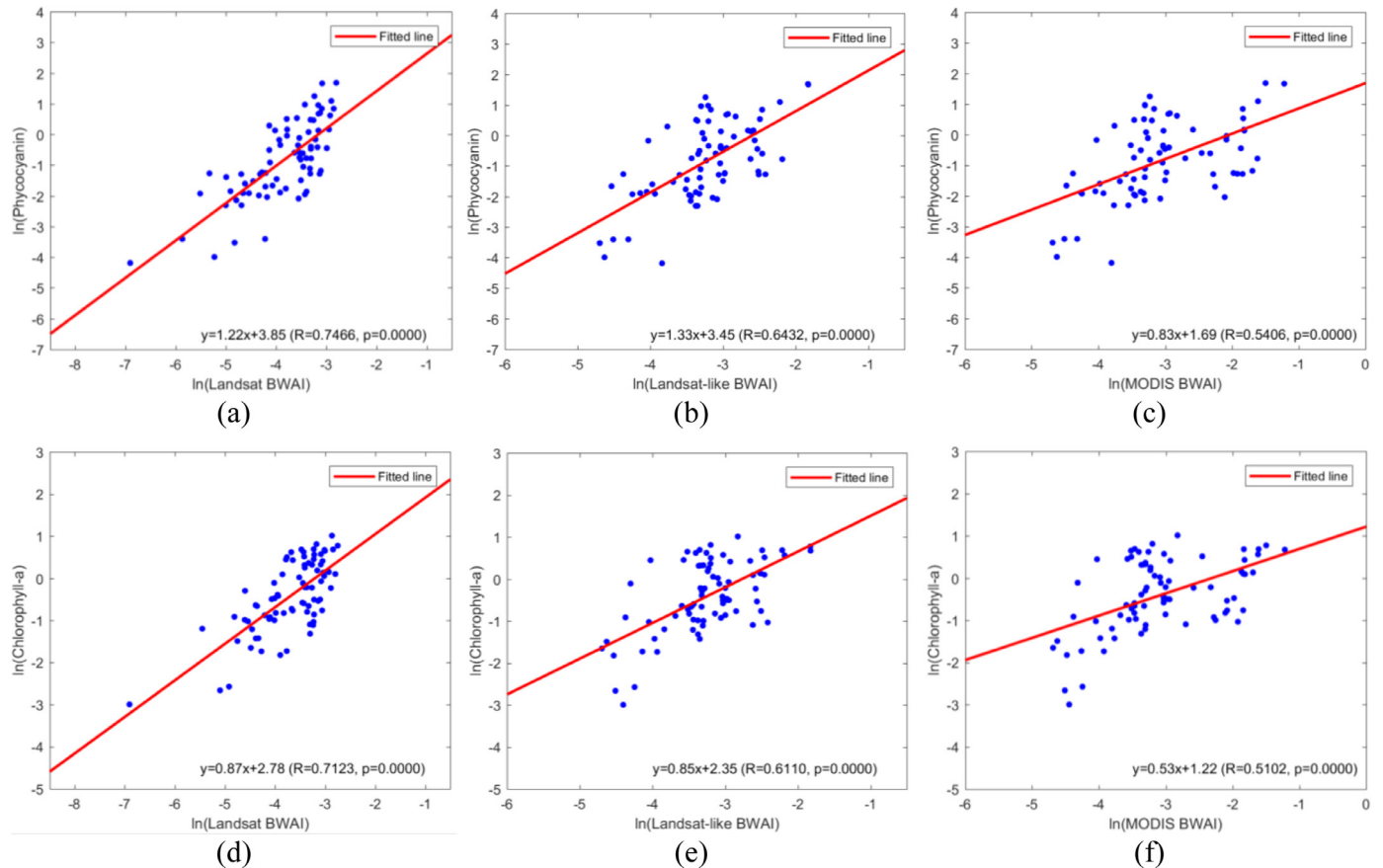


**Fig. 15.** The scatter plots between the  $BWAI_L$ ,  $BWAI_{L'}$ , and  $BWAI_M$  (X-axis) and the log-transformed *in situ* PC and Chl-a concentrations (Y-axis) on the 16 dates in Table A1 of the Appendix.

## Appendix A

**Table A1**

The availability of the *in situ* and Landsat data on the 16 dates in 2017 for the quantitative evaluation of CyanoHAB index development and fusion.

Date	lemrbhd	osugi	tolcrib	utlcp	bgsusd	bgsusd2	bgsdb	WE2	WE4	WE8	WE13	leorgn	ETM+	OLI
Jul. 08	•	•	•	•	•	•		•	•	•	•	•		•
Jul. 09	•	•	•	•	•	•		•	•	•	•	•	•	
Jul. 16	•	•	•	•	•	•		•	•	•	•	•		
Jul. 17	•	•	•	•	•	•		•	•	•	•	•		
Jul. 25	•	•	•	•	•	•		•	•	•	•	•		
Aug. 01	•	•	•	•	•	•		•	•	•	•	•		
Aug. 02	•	•	•	•	•	•		•	•	•	•	•		
Aug. 09	•	•	•	•	•	•		•	•	•	•	•		
Aug. 10	•	•	•	•	•	•		•	•	•	•	•		
Aug. 25	•	•	•	•	•	•		•	•	•	•	•		
Aug. 26	•	•	•	•	•	•		•	•	•	•	•		
Sep. 03	•	•	•	•	•	•		•	•	•	•	•		
Sep. 10	•	•	•	•	•	•		•	•	•	•	•		
Sep. 26	•	•	•	•	•	•		•	•	•	•	•		
Oct. 05	•	•	•	•	•	•		•	•	•	•	•		
Oct. 20	•	•	•	•	•	•		•	•	•	•	•		

## References

- Anderson, D.M., Glibert, P.M., Burkholder, J.M., 2002. Harmful algal blooms and eutrophication: nutrient sources, composition, and consequences. *Estuaries* 25, 704–726.
- Babin, M., Roesler, C.S., Cullen, J.J., 2008. Real-time Coastal Observing Systems for Marine Ecosystem Dynamics and Harmful Algal Blooms: Theory, Instrumentation and Modelling. UNESCO.
- Cammalleri, C., Anderson, M., Gao, F., Hain, C., Kustas, W., 2013. A data fusion approach for mapping daily evapotranspiration at field scale. *Water Resour. Res.* 49, 4672–4686.
- Clark, J.M., Schaeffer, B.A., Darling, J.A., Urquhart, E.A., Johnston, J.M., Ignatius, A.R., Myer, M.H., Loftin, K.A., Werdell, P.J., Stumpf, R.P., 2017. Satellite monitoring of cyanobacterial harmful algal bloom frequency in recreational waters and drinking water sources. *Ecol. Indic.* 80, 84–95.
- Dona, C., Chang, N.-B., Caselles, V., Sánchez, J.M., Camacho, A., Delegido, J., Vanah, B.W., 2015. Integrated satellite data fusion and mining for monitoring lake water quality status of the Albufera de Valencia in Spain. *J. Environ. Manag.* 151, 416–426.
- Galat, D.L., Verdin, J.P., 1989. Patchiness, collapse and succession of a cyanobacterial bloom evaluated by synoptic sampling and remote sensing. *J. Plankton Res.* 11, 925–948.
- Gao, F., Hilker, T., Zhu, X., Anderson, M., Masek, J., Wang, P., Yang, Y., 2015. Fusing Landsat and MODIS data for vegetation monitoring. *IEEE Geosci. Remote Sens. Mag.* 3, 47–60.
- Gao, F., Masek, J., Schwaller, M., Hall, F., 2006. On the blending of the Landsat and MODIS surface reflectance: predicting daily Landsat surface reflectance. *IEEE Trans. Geosci. Remote Sens.* 44, 2207–2218.
- Gevaert, C.M., García-Haro, F.J., 2015. A comparison of STARFM and an unmixing-based algorithm for Landsat and MODIS data fusion. *Remote Sens. Environ.* 156, 34–44.
- Gitelson, A., 1993. Algorithms for remote sensing of phytoplankton pigments in inland waters. *Adv. Space Res.* 13, 197–201.
- Gitelson, A., Garbuзов, G., Szilagyi, F., Mittenzwey, K., Karniel, A., Kaiser, A., 1993. Quantitative remote sensing methods for real-time monitoring of inland waters quality. *Int. J. Remote Sens.* 14, 1269–1295.
- Glibert, P.M., Anderson, D.M., Gentien, P., Granéli, E., & Sellner, K.G. (2005). The Global, Complex Phenomena of Harmful Algal Blooms
- Goodin, D.G., Han, H.L., Fraser, R.N., Rundquist, D.C., Stebbins, W.A., Schalles, J., 1993. Analysis of suspended solids in water using remotely sensed high resolution derivative spectra. *Photogramm. Eng. Remote Sens.* 59, 505–510.
- Gower, J., 1980. Observations of *in situ* fluorescence of chlorophyll-A in Saanich inlet. *Bound. Layer Meteorol.* 18, 235–245.
- Gower, J., King, S., Borstad, G., Brown, L., 2005. Detection of intense plankton blooms using the 709 nm band of the MERIS imaging spectrometer. *Int. J. Remote Sens.* 26, 2005–2012.
- Hagolle, O., Huc, M., Pascual, D.V., Dedieu, G., 2010. A multi-temporal method for cloud detection, applied to FORMOSAT-2, VENµS, LANDSAT and SENTINEL-2 images. *Remote Sens. Environ.* 114, 1747–1755.
- Hallegraeff, G.M., 1993. A review of harmful algal blooms and their apparent global increase. *Phycologia* 32, 79–99.
- Ho, J., Michalak, A., Pahlevan, N., 2019. Widespread global increase in intense lake phytoplankton blooms since the 1980s. *Nature* 1-1.
- Ho, J.C., Michalak, A.M., 2015. Challenges in tracking harmful algal blooms: a synthesis of evidence from Lake Erie. *J. Great Lakes Res.* 41, 317–325.
- Ho, J.C., Stumpf, R.P., Bridgeman, T.B., Michalak, A.M., 2017. Using Landsat to extend the historical record of lacustrine phytoplankton blooms: a Lake Erie case study. *Remote Sens. Environ.* 191, 273–285.
- Hu, C., 2009. A novel ocean color index to detect floating algae in the global oceans. *Remote Sens. Environ.* 113, 2118–2129.
- Hu, C., Lee, Z., Franz, B., 2012. Chlorophyll algorithms for oligotrophic oceans: a novel approach based on three-band reflectance difference. *J. Geophys. Res. Oceans* 117.
- Hu, C., Lee, Z., Ma, R., Yu, K., Li, D., Shang, S., 2010. Moderate resolution imaging spectroradiometer (MODIS) observations of cyanobacteria blooms in Taihu Lake, China. *J. Geophys. Res. Oceans* 115.
- Huang, B., Zhang, H., 2014. Spatio-temporal reflectance fusion via unmixing: accounting for both phenological and land-cover changes. *Int. J. Remote Sens.* 35, 6213–6233.
- Huang, B., Zhao, Y., 2017. Research status and prospect of spatiotemporal fusion of multi-source satellite remote sensing imagery. *Acta Geod. Cartogr. Sin.* 46, 1492.
- Jarihani, A., McVicar, T., Van Niel, T., Emelyanova, I., Callow, J., Johansen, K., 2014. Blending Landsat and MODIS data to generate multispectral indices: a comparison of “Index-then-Blend” and “Blend-then-Index” approaches. *Remote Sens.* 6, 9213–9238.
- Jiang, H., Shen, H., Li, X., Zeng, C., Liu, H., Lie, F., 2019. Extending the SMAP 9-km soil moisture product using a spatio-temporal fusion model. *Remote Sens. Environ.* 231, 11122.
- Kahru, M., Sachuk, O., Elmgren, R., 2007. Satellite measurements of cyanobacterial bloom frequency in the Baltic Sea: interannual and spatial variability. *Marine Ecol. Prog. Ser.* 343, 15–23.
- Kutser, T., 2004. Quantitative detection of chlorophyll in cyanobacterial blooms by satellite remote sensing. *Limnol. Oceanogr.* 49, 2179–2189.
- Kutser, T., 2009. Passive optical remote sensing of cyanobacteria and other intense phytoplankton blooms in coastal and inland waters. *Int. J. Remote Sens.* 30, 4401–4425.
- Kutser, T., Metsamaa, L., Vahtmäe, E., Strömbbeck, N., 2006. Suitability of MODIS 250 m resolution band data for quantitative mapping of cyanobacterial blooms. *Proc. Estonian Acad. Sci. Biol. Ecol.* 55, 318–328.
- Lathrop, R., 1992. Landsat thematic mapper monitoring of turbid inland water quality. *Photogramm. Eng. Remote Sens.* 58, 465–470.
- Letelier, R.M., Abbott, M.R., 1996. An analysis of chlorophyll fluorescence algorithms for the moderate resolution imaging spectrometer (MODIS). *Remote Sens. Environ.* 58, 215–223.
- Levy, R., Mattoe, S., Munchak, L., Remer, L., Sayer, A., Patadia, F., Hsu, N., 2013. The collection 6 MODIS aerosol products over land and ocean. *Atmos. Meas. Tech.* 6, 2989.
- Lunetta, R.S., Schaeffer, B.A., Stumpf, R.P., Keith, D., Jacobs, S.A., Murphy, M.S., 2015. Evaluation of cyanobacteria cell count detection derived from MERIS imagery across the eastern USA. *Remote Sens. Environ.* 157, 24–34.
- Lyapustin, A., Wang, Y., Xiong, X., Meister, G., Platnick, S., Levy, R., Franz, B., Korkin, S., Hilker, T., Tucker, J., 2014. Scientific impact of MODIS C5 calibration degradation and C6+ improvements. *Atmos. Meas. Tech.* 7, 4353–4365.
- Matthews, M.W., 2011. A current review of empirical procedures of remote sensing in inland and near-coastal transitional waters. *Int. J. Remote Sens.* 32, 6855–6899.
- Matthews, M.W., Bernard, S., Robertson, L., 2012. An algorithm for detecting trophic status (chlorophyll-a), cyanobacterial-dominance, surface scums and floating vegetation in inland and coastal waters. *Remote Sens. Environ.* 124, 637–652.
- Mayo, M., Gitelson, A., Yacobi, Y., Ben-Avraham, Z., 1995. Chlorophyll distribution in Lake Kinneret determined from Landsat thematic mapper data. *Remote Sens.* 16, 175–182.
- Mertes, L.A., Smith, M.O., Adams, J.B., 1993. Estimating suspended sediment concentrations in surface waters of the Amazon River wetlands from Landsat images. *Remote Sens. Environ.* 43, 281–301.
- Michalak, A.M., Anderson, E.J., Beletsky, D., Boland, S., Bosch, N.S., Bridgeman, T.B., Chaffin, J.D., Cho, K., Confesor, R., Daloglu, I., 2013. Record-setting algal bloom in Lake Erie caused by agricultural and meteorological trends consistent with expected future conditions. *Proc. Natl. Acad. Sci.* 110, 6448–6452.
- Mishra, S., Mishra, D.R., 2012. Normalized difference chlorophyll index: a novel model for remote estimation of chlorophyll-a concentration in turbid productive waters. *Remote Sens. Environ.* 117, 394–406.
- Nechad, B., Ruddick, K., Park, Y., 2010. Calibration and validation of a generic multisensor algorithm for mapping of total suspended matter in turbid waters. *Remote Sens. Environ.*, 114, 854–866.
- NOAA (2019). Harmful Algal Blooms in Lake Erie - Experimental and Operational HAB Bulletin Archive. Retrieved November 01, 2019, from [https://www.glerl.noaa.gov/res/HABs\\_and\\_Hypoxia/lakeErieHABArchive/](https://www.glerl.noaa.gov/res/HABs_and_Hypoxia/lakeErieHABArchive/).
- ODNR (2016). Lake Erie Facts. Retrieved July 31, 2019, from <http://geosurvey.ohiodnr.gov/lake-erie-geology/facts>.
- Oyama, Y., Matsushita, B., Fukushima, T., 2015. Distinguishing surface cyanobacterial blooms and aquatic macrophytes using Landsat/TM and ETM+ shortwave infrared bands. *Remote Sens. Environ.* 157, 35–47.
- Philpot, W.D., 1991. The derivative ratio algorithm: avoiding atmospheric effects in remote sensing. *IEEE Trans. Geosci. Remote Sens.* 29, 350–357.
- Reutter, J. (2014). Harmful Algal Bloom Q&A and Updates. Retrieved September 25, 2019, from <https://ohioseagrant.osu.edu/news/2014/a8990/harmful-algal-bloom-q-updates>.
- Ritchie, J.C., Schieber, F.R., McHenry, J.R., 1976. Remote sensing of suspended sediments in surface waters. *Photogramm. Eng. Remote Sens.* 42, 1539–1545.
- Ritchie, J.C., Zimba, P.V., Everitt, J.H., 2003. Remote sensing techniques to assess water quality. *Photogramm. Eng. Remote Sens.* 69, 695–704.
- Simis, S.G., Peters, S.W., Gons, H.J., 2005. Remote sensing of the cyanobacterial pigment phycocyanin in turbid inland water. *Limnol. Oceanogr.* 50, 237–245.
- Stumpf, R.P., Davis, T.W., Wynne, T.T., Graham, J.L., Loftin, K.A., Johengen, T.H., Gossiaux, D., Palladino, D., Burtner, A., 2016. Challenges for mapping cyanotoxin patterns from remote sensing of cyanobacteria. *Harmful Algae* 54, 160–173.
- Stumpf, R.P., Werdell, P.J., 2010. Adjustment of ocean color sensor calibration through multi-band statistics. *Opt. Express* 18, 401–412.
- Swain, R., Sahoo, B., 2017. Mapping of heavy metal pollution in river water at daily time-scale using spatio-temporal fusion of MODIS-aqua and Landsat satellite imageries. *J. Environ. Manag.* 192, 1–14.
- Twardowski, M.S., Boss, E., Sullivan, J.M., Donaghay, P.L., 2004. Modeling the spectral shape of absorption by chromophoric dissolved organic matter. *Mar. Chem.* 89, 69–88.
- Vincent, R.K., Qin, X., McKay, R.M.L., Miner, J., Czajkowski, K., Savino, J., Bridgeman, T., 2004. Phycocyanin detection from LANDSAT TM data for mapping cyanobacterial blooms in Lake Erie. *Remote Sens. Environ.* 89, 381–392.
- Wang, M., Shi, W., 2007. The NIR-SWIR combined atmospheric correction approach for MODIS ocean color data processing. *Opt. Express* 15, 15722–15733.
- Wang, Z., Bovik, A.C., Sheikh, H.R., Simoncelli, E.P., 2004. Image quality assessment: from error visibility to structural similarity. *IEEE Trans. Image Process.* 13, 600–612.
- Weng, Q., Fu, P., Gao, F., 2014. Generating daily land surface temperature at Landsat resolution by fusing Landsat and MODIS data. *Remote Sens. Environ.* 145, 55–67.
- Wulder, M.A., Loveland, T.R., Roy, D.P., Crawford, C.J., Masek, J.G., Woodcock, C.E., Allen, R.G., Anderson, M.C., Belward, A.S., Cohen, W.B., 2019. Current status of Landsat program, science, and applications. *Remote Sens. Environ.* 225, 127–147.
- Wynne, T., Stumpf, R., Briggs, T., 2013. Comparing MODIS and MERIS spectral shapes for cyanobacterial bloom detection. *Int. J. Remote Sens.* 34, 6668–6678.
- Wynne, T., Stumpf, R., Tomlinson, M., Warner, R., Tester, P., Dyble, J., Fahnestiel, G., 2008. Relating spectral shape to cyanobacterial blooms in the Laurentian Great Lakes. *Int. J. Remote Sens.* 29, 3665–3672.
- Wynne, T.T., Stumpf, R.P., Tomlinson, M.C., Warner, R., Tester, P., Dyble, J., Fahnestiel, G., 2010. Characterizing a cyanobacterial bloom in western Lake Erie using satellite imagery and meteorological data. *Limnol. Oceanogr.* 55, 2025–2036.
- Xu, H., 2006. Modification of normalised difference water index (NDWI) to enhance open water features in remotely sensed imagery. *Int. J. Remote Sens.* 27, 3025–3033.
- Yacobi, Y.Z., Gitelson, A., Mayo, M., 1995. Remote sensing of chlorophyll in Lake Kinneret using high-spectral-resolution radiometer and Landsat TM: spectral features of reflectance and algorithm development. *J. Plankton Res.* 17, 2155–2173.
- Zhang, M., 2015. Estimating Aerosol Concentrations Over the Pearl River Delta Region Using Satellite Remote Sensing Techniques. The Chinese University of Hong Kong (Hong Kong).

- Zhao, Y., Huang, B., 2017. A hybrid image fusion model for generating high spatial-temporal-spectral resolution data using OLI-MODIS-hyperion satellite imagery. *World Acad. Sci. Eng. Technol. Int. J. Environ. Chem. Ecol. Geol. Geophys. Eng.* 11, 843–848.
- Zhao, Y., Huang, B., Marinoni, A., Gamba, P., 2018a. High spatiotemporal resolution PM2.5 concentration estimation with satellite and ground observations: a case study in New York City. In: Proceedings of the IEEE International Conference on Environmental Engineering (IEE). IEEE, pp. 1–5.
- Zhao, Y., Huang, B., Song, H., 2018b. A robust adaptive spatial and temporal image fusion model for complex land surface changes. *Remote Sens. Environ.* 208, 42–62.
- Zhou, L., Divakarla, M., Liu, X., Layns, A., Goldberg, M., 2019. An overview of the science performances and calibration/validation of joint polar satellite system operational products. *Remote Sens.* 11, 698.
- Zhu, X., Chen, J., Gao, F., Chen, X., Masek, J.G., 2010. An enhanced spatial and temporal adaptive reflectance fusion model for complex heterogeneous regions. *Remote Sens. Environ.* 114, 2610–2623.
- Zhu, X., Helmer, E.H., Gao, F., Liu, D., Chen, J., Lefsky, M.A., 2016. A flexible spatiotemporal method for fusing satellite images with different resolutions. *Remote Sens. Environ.* 172, 165–177.